UNIVERSIDAD DE CHILE
FACULTAD DE CIENCIAS FÍSICAS Y MATEMÁTICAS
DEPARTAMENTO DE INGENIERÍA CIVIL

ESTIMATION OF EMPIRICAL RESPONSE SPECTRUM AND LOCAL RESPONSES OF THE JUSTICIA ESPADA ACUÑA MENA BUILDING USING THE MOD-Z(VAR) METHOD FOR THE 2010 CENTRAL CHILEAN MEGA-EARTHQUAKE (MW=8.8)

TESIS PARA OPTAR AL GRADO DE MAGÍSTER EN CIENCIAS DE LA INGENIERÍA, MENCIÓN INGENIERÍA ESTRUCTURAL, SÍSMICA Y GEOTÉCNICA

MEMORIA PARA OPTAR AL TÍTULO DE INGENIERO CIVIL

BENJAMÍN ANDRÉS ARELLANO SANDOVAL

PROFESOR GUÍA:

FRANCISCO HERNÁNDEZ PRADO

MIEMBROS DE LA COMISIÓN:

LEONARDO MASSONE SÁNCHEZ

RODRIGO ASTROZA EULUFÍ

SANTIAGO DE CHILE

2023

RESUMEN DE LA TESIS PARA OPTAR AL GRADO DE: MAGÍSTER EN CIENCIAS DE LA INGENIERÍA, MENCIÓN INGENIERÍA ESTRUCTURAL, SÍSMICA Y GEOTÉCNICA
MEMORIA PARA OPTAR AL TÍTULO DE: INGENIERO CIVIL
POR: BENJAMÍN ANDRÉS ARELLANO SANDOVAL
FECHA: 2023
PROFESOR GUÍA: FRANCISCO HERNÁNDEZ PRADO

ESTIMACIÓN DE ESPECTROS DE RESPUESTA EMPÍRICOS Y RESPUESTAS LOCALES DEL EDIFICIO JUSTICIA ESPADA ACUÑA MENA MEDIANTE EL MÉTODO MOD-Z(VAR) PARA EL MEGATERREMOTO DE CHILE CENTRAL DE 2010 (MW=8.8)

En el presente trabajo se formula, implementa y valida una nueva técnica de identificación de sistemas llamada Mod-ζ (var) para estudiar la respuesta sísmica de un edificio de muros de corte 3D de hormigón armado durante el megaterremoto de Chile central de 2010 (Mw=8.8). El enfoque Mod-ζ(var) es una evolución de las técnicas de identificación del sistema modal de mínimos cuadrados, donde los parámetros modales se ajustan a través de pequeñas ventanas de datos para adaptarse a los datos sísmicos en los dominios de frecuencia y tiempo. Esta técnica ofrece varias ventajas sobre los métodos tradicionales, incluida la estimación de propiedades dinámicas variables en el tiempo durante eventos sísmicos y la evaluación confiable de respuestas modales no lineales continuas. Como resultado, el método Mod-ζ(var) permite la determinación de espectros de respuesta empíricos relacionados con cada entrada sísmica. El método también puede calcular la respuesta local de pisos medidos y no medidos como el producto entre las respuestas modales no lineales (obtenidas del enfoque Mod-ζ(var)) y las formas modales normalizadas sísmicas para todos los pisos de edificios (que se pueden estimar a partir de datos de vibraciones ambientales). Finalmente, las deformaciones sísmicas de piso se pueden imponer en un FEM para determinar cantidades ingenieriles relevantes, como las derivas entre pisos, las fuerzas entre pisos y la demanda local de elementos estructurales (por ejemplo, derivas, curvaturas, fuerzas internas, tensiones, deformaciones).

***Palabras claves**: Espectro de Respuesta Empírico, Respuesta Sísmica Local, Respuesta de Pisos no Medidos, Método Mod-ζ (var), Propiedades Dinámicas Variables en el Tiempo.*

ESTIMATION OF EMPIRICAL RESPONSE SPECTRUM AND LOCAL RESPONSES OF THE JUSTICIA ESPADA ACUÑA MENA BUILDING USING THE MOD-ζ(VAR) METHOD FOR THE 2010 CENTRAL CHILEAN MEGA-EARTHQUAKE (Mw=8.8)

Benjamín Arellano[1], Francisco Hernández[1], Leonardo M. Massone[1], Rodrigo Astroza[2], Pedro Soto[1], Nicolás Contreras[3], Bastián Garrido[1]

[1] Department of Civil Engineering, University of Chile, Av. Blanco Encalada 2002, Santiago, Chile

[2] Facultad de Ingeniería y Ciencias Aplicadas, Universidad de los Andes, Monseñor Álvaro del Portillo Nº12.455, Las Condes, Santiago, Chile

[3] Centre for Infraestructural Monitoring and Protection, School of Civil and Mechanical Engineering, Curtin University, Australia.

ABSTRACT

A novel system identification technique called Mod-ζ (var) is formulated, implemented, and validated to study the seismic response of a 3D R/C shear wall building during the 2010 central Chilean mega-earthquake (Mw=8.8). The Mod-ζ(var) approach is an evolution of Least-Square modal system identification techniques, where modal parameters are adjusted through small data windows to fit seismic data in the frequency and time domains. This technique offers several advantages over traditional methods, including the estimation of time-variant dynamic properties during seismic events and the reliable assessment of continuous nonlinear modal responses. As a result, the Mod-ζ(var) approach allows for the determination of empirical response spectra related to each seismic input. The technique can also compute the local response of measured and unmeasured floors as the product between the nonlinear modal responses (obtained from the Mod-ζ(var) approach) and the normalized seismic mode shapes for all building floors (which can be estimated from ambient vibration data). Finally, the seismic floor deformations can be imposed on a FEM to determine relevant engineering quantities such as inter-story drift, inter-story forces, and local demand of structural elements (e.g., drifts, curvatures, internal forces, stresses, strains)**.**

Keywords*: Empirical Response Spectrum, Local Seismic Response, Unmeasured Floor Responses, Mod-ζ (var) Approach, Time-Variant Dynamic Properties*

AGRADECIMIENTOS

Mi más sincero agradecimiento a mis grandes amados padres, Lilian y Andrés, por todo el apoyo que me han dado, por la ayuda que me han brindado, por su amor incondicional, por hacer de mis logros suyos, por todo el esfuerzo y sacrificio que han dado por mi y mi hermana, me siento muy orgulloso de tenerlos como padres. También extiendo un agradecimiento especial a mi hermana Camila, quien siempre ha sido fuente de inspiración para mí, un ejemplo a seguir, te amo mucho manita, gracias por creer en mí.

Estoy agradecido por todas las amistades que formé durante mi educación universitaria que van más allá del ámbito académico. A mi grupo de amigos Clansito que conocí en mis primeros años universitarios, gracias por aquellos buenos momentos, por todas las risas y el apoyo que me dieron. A mi grupo de amigos de especialidad los Copuchentos, por todas esas tardes de estudios, las celebraciones cumpleañeras y el cariño que han entregado. En especial agradecer a mi amigo del alma Matías Céspedes. Fuimos compañeros de puesto en el INBA, luego entramos a Ingeniería quedando ambos en la sección 7 y finalmente terminamos en la misma especialidad. Gracias por apoyarme en los altibajos de la vida.

Expreso mi agradecimiento por haber conocido a Daniela Sánchez, la polola más maravillosa que uno podría desear. Gracias por tu amistad, por la confianza, por la felicidad, por el apoyo y amor que me das. Fuiste un pilar fundamental durante mi proceso tesis, tu aliento y confianza en mi me ayudaron en todo momento. Te amo mucho.

Finalmente quiero expresar mis agradecimientos a las personas que han contribuido en mi crecimiento profesional. En primer lugar, agradezco al profesor Francisco Hernández por su compromiso con los estudiantes y su enseñanza, por su vocación como docente y académico, por su paciencia, guía y apoyo durante este proceso de cierre universitario. Además, me gustaría agradecer a los profesores Rafael Ruiz, Juan Felipe Beltrán y Ricardo Herrera, quienes, junto al profesor Hernández, me brindaron la oportunidad de trabajar con ellos durante varios semestres y fomentar mi pasión por la docencia, en donde espero haber podido aportar en el desarrollo profesional de los estudiantes.

Table of Content

1. INTRODUCTION

The system identification (SI) of structures is an inverse problem that attempts to estimate the structure's characteristics and the global/local responses from measured data. To sum up, SI focuses on determining the dynamic properties, monitoring the structural health, and studying the actual seismic performances of structures from recorded data obtained from sensors installed on them. Different SI techniques are employed depending on the kind of excitations or input signals. In this context, several MIMO (Multiple Inputs - Multiple Outputs) SI techniques can be applied to estimate the dynamic properties of linear systems when the structure is subjected to consecutive impact tests, seismic excitations, or harmonic loads (i.e., when input and output signals are simultaneously recorded). Between them, the Deterministic Stochastic Identification (DSI) method [1,2], the Complex-Mode Indicator Function [3], the multivariable Output-Error State Space (MOESP) algorithm [4], the Auto Regressive with external input ARX method [5], ARX with moving average ARMAX [6], the Eigensystem Realization Algorithm applied to the response impulse obtained from the Observed/Kalman Filter Identification OKID/ERA method [7,8], the System Realization using Information Matrix method (SRIM) [9,10], Least-Square (LS) Output-error methods in the time domain [11,12] and also in the frequency domain [13], neural network models [14], Frequency Response Functions (FRF) methods such as the frequency domain poly reference modal analysis method [15], interferometry techniques based on the wave propagation theory [16], can be identified.

MIMO techniques work accurately for linear structures with small deformations, but their accuracy decreases when systems experience nonlinearities due to various factors, such as nonlinear responses of structural elements, interactions with nonstructural components, and Soil-Foundation-Structure-Interaction, among others. SI techniques assume linear-elastic behavior or provide an average estimation of dynamic properties, which leads to inaccurate model-predicted responses when dynamic properties vary over time. Additionally, model-predicted responses can only be evaluated at sensor positions. On the other hand, MIMO SI techniques can still be used for nonlinear systems assuming linear behavior through small data windows. For example, the Short-Time DSI (STDSI) technique estimates time-variant natural frequencies of the BNCS building [17], though damping ratios may become particularly noisy.

Similarly, a calibrated FEM that simulates the nonlinear response of the principal structural elements can be employed to estimate local/global responses that are not directly measured by sensors. This process has been made manually or by using sophisticated techniques based on optimization tools [18], maximum-likelihood techniques [19], recursive least-squares [20,21], the recursive instrumental-variable method [4], Bayesian approaches or Kalman filters [22]. These model-based approaches have been successful for simple structures whose dynamic response can be appropriately modeled based on a few numbers of linear or nonlinear elements that mainly describe its seismic response. However, they could be highly inaccurate for large and complex real-life structures, where several nonlinear effects cannot be adequately simulated. Another family of SI techniques is biologically-inspired (BI)

methods such as Neural Networks [23–29], Genetic Algorithms [30–33], or particle swarm optimizations [34]. However, the accuracy of the BI depends on how the model is trained. For example, the trained algorithm can become inaccurate when it is employed to extrapolate results related to a new set of data that is out of the training range. They are black-box processes that are not necessarily related to the physical phenomenon, and their interpretation can become complex. Finally, several time-frequency representations have been proposed to evaluate the time-variant frequencies contained in a signal, such as a Spectrogram [35], the Wigner-Ville distribution [35], the Hilbert-Huang transform [36], the Wavelet transform [37], the Short-Time-Transfer-Function [17,38] and the Short-Time-Seismic-Frequency-Decomposition [39]. These practical tools provide a graphical representation of how the predominant frequencies of the signal can vary over time. However, they do not allow direct estimation of how other dynamic properties change (mode shapes or damping ratios) or evaluate different relevant seismic engineering quantities for understating the structure's behavior.

A promising SI technique called Mod-ζ (var) approach (Section 2) that can be employed for linear or nonlinear structures subjected to seismic loads was previously formulated and implemented by Hernández et al. [40,41]. This technique has effectively tracked how the dynamic properties of a 2D structure shift during seismic events. The Mod-ζ (var) approach is a least-square (LS) approach that fits time-variant modal parameters so that the model-predicted response matches measured seismic data, for all channels, in the time and frequency domains. It assumes nonlinear SDOF modal responses that are computed from time-variant dynamic properties, which are consequently adjusted by small data windows. Therefore, the Mod-ζ (var) approach is a modal-parametric LS approach that can be understood as an evolution of the LS modal-parametric methods suggested by Beck [12], Li and Mau [11], or Carreño [42,43]. For example, Carreño [42,43] presented a similar LS modal parametric approach that refers to an optimization problem that minimizes the weighted quadratic error between the measured seismic data and the model-predicted response computed as the superposition of multiple modal responses. Likewise, it assumes constant dynamic properties over small data windows, which implies discontinuous modal parameters between consecutive data windows, generating discontinuous modal responses.

The Mod-ζ (var) approach's advantages in comparison to previous modal LS methods can be summarized as follows: i) it employs a numeric constant acceleration method to solve the nonlinear modal SDOF responses, ii) it uses modal parameters that change each time step during each data window rather than assume constant modal parameters through small data windows, iii) it employs seismic normalized mode shapes (that implies that the SDOF response is the modal response directly) that allows restraining their combined variations because their sum should remain constant and equal to the seismic influence vector (allowing disaggregating mode shapes variations from damping ratios fluctuations), iv) it fits all mode responses simultaneously rather than including each modal response incrementally, v) model-predicted and modal responses become continuous functions, avoiding discontinuous modal responses that occur between consecutive data windows when modal parameters are assumed constant during each data window. In summary, the novelty of the Mod-ζ (var)

approach resides in that it allows for estimating the time-variant dynamic properties that are continuous functions over the entire seismic record. This methodology has been successfully applied to a 2D building tested on a one-directional shake table by Hernandez et al. [40,41]. Results showed that the Mod-ζ (var) approach was practical to analyze the seismic response of a small-scale 5-DOF steel frame structure with attached nonlinear energy dissipation devices. In particular, the method offered a high resolution for estimating time-variant damping ratios, i.e., a helpful tool for comparing the dissipation capacities provided by different damper-cable-pulley systems installed into the tested structure. Moreover, the method allowed obtaining the empirical response spectrum and other relevant engineering quantities, such as inter-story drift or shear forces, which were compared between different tested configurations.

As mentioned, the Mod-ζ (var) method is a SI technique that has provided accurate results for 2D nonlinear reduced-scale limited-DOF cases. However, this approach has not yet been applied to large 3D real-scale buildings. For this reason, the manuscript aims to extend the method to account for 3D mode shapes and consider multiple seismic inputs. The upgraded method is validated against simulate data of a FEM model and measured records of the Justicia Espada Acuña Mena (JEAM) building allocated inside the Faculty of Physic and Mathematics of the University of Chile in Santiago, Chile. It is worth noting that the JEAM building has had a local net of unidirectional accelerometers since 2009, which has allowed the recording of multiple seismic events, including the Chilean mega-earthquake of 27 February 2010 (Mw=8.8), where the JEAM building experienced low structural damage. The manuscript is structured as follows: section 2 presents the theoretical basis of the upgraded 3D method. In section 3, the case study is described. Section 4 identifies the natural frequencies and mode shapes of the JEAM building using Operational Modal Analysis (OMA). Section 5 introduces a linear FEM model of the JEAM building, and its seismic response is computed and employed to validate the Mod-ζ (var) method. Section 6 applies the Mod-ζ (var) method to evaluate the seismic data recorded by the seismic instrumentation of the JEAM building during the central Chilean mega-earthquake (Mw=8.8), allowing estimating the empirical response spectra. Finally, section 7 combines the SDOF modal responses obtained from the Mod-ζ (var) method with seismic normalized mode shapes estimated from OMA to determine global and local responses of the building.

2. MOD- Z(VAR) METHOD FOR THE MIMO 3D CASE

The principles of the Mod-ζ(var) method applied to a 2D MDOF structure subjected to a single horizontal seismic input (SIMO - Single Input Multiple Outputs) were detailed by Hernandez et al. [40,41]. This article expands the Mod-ζ(var) approach for 3D systems subjected to multiple seismic inputs. Hence, the seismic response for the MIMO case is obtained by the superposition between the seismic response computed for each seismic input (SIMO), even when the structure behaves nonlinearly. Similarly, longitudinal, transverse, and torsional responses are included by considering 3D mode shapes. The Mod-ζ(var) method refers to a parametric method where the time-variant modal parameters are adjusted by small data windows using optimization tools (fmincon function available in MATLAB).

The objective is to minimize the difference between the measured and model-predicted responses by small data windows. The MDOF model-predicted seismic response subjected to multiple seismic inputs (MIMO) is computed as follows,

$$\ddot{\mathbf{u}}_t\left(t_k\right) \approx \sum_{j=1}^{I}\left(\sum_{i=1}^{N_2}\boldsymbol{\varphi}_{ij}\left(t_k\right)\cdot\ddot{Y}_{ij}\left(t_k\right)+\tilde{\mathbf{r}}_j\cdot\ddot{v}_j^g\left(t_k\right)\right) \quad (1)$$

Where $\ddot{\mathbf{u}}_t\left(t_k\right)=\left(\ddot{u}_t^1\left(t_k\right),\ddot{u}_t^2\left(t_k\right),...,\ddot{u}_t^{N_m}\left(t_k\right)\right)=$ is the absolute acceleration response related to the measured DOFs ($N_m\times 1$) (the symbol ~ refers to N_m measured DOFs), $\boldsymbol{\varphi}_{ij}\left(t_k\right)=$ the seismic normalized mode shape associated with the i-th mode response, and the j-th seismic input for the measured DOFs, ($N_m\times 1$) $\ddot{Y}_{ij}\left(t_k\right)=$the relative acceleration response associated with the i-th mode response and the j-th seismic input, $\tilde{\mathbf{r}}_j=$ the influence seismic vector at the measured DOFs related to the j-th seismic input, $\ddot{v}_j^g\left(t_k\right)=$ the j-th acceleration seismic input, $N_2=$the number of modes considered into the solution, $N=$the number of DOFs or mode shapes of the system, $I=$the number of seismic inputs. It must be noted that the relative responses associated with $N-N_2$ structural modes can be ignored because of their low seismic participation (or because they were previously eliminated using low-pass frequency filters applied to the inputs and outputs signals, respectively).

"The normalized seismic mode shape has an explicit physical meaning. The seismic normalized mode shape values indicate how significant the response can be on the dynamic response of the analyzed DOF for a specific structural mode, i.e., it refers to the amplification that the DOF experience compared to the modal SDOF response (e.g., a value of one implies that the DOF behaves identically to an SDOF system). Moreover, the sign of each DOFs represents physically if the DOF is tuned or untuned with the SDOF modal response" [40]. This explanation is also applicable in the case of multiple seismic inputs (MI) without missing generalization. Overall, seismic normalized mode shapes can be computed from the mass matrix ($\mathbf{M}$) and a group of not-normalized mode shapes $\boldsymbol{\psi}_j\left(t_k\right)$ as follows,

$$\boldsymbol{\varphi}_{ij}\left(t_k\right)=\boldsymbol{\psi}_i\left(t_k\right)\cdot\frac{\boldsymbol{\psi}_i\left(t_k\right)^T\cdot\mathbf{M}\cdot\mathbf{r}_j}{\boldsymbol{\psi}_i\left(t_k\right)^T\cdot\mathbf{M}\cdot\boldsymbol{\psi}_i\left(t_k\right)}=\boldsymbol{\psi}_i\left(t_k\right)\cdot\alpha_{ij}\left(t_k\right)\Rightarrow\frac{\boldsymbol{\varphi}_i\left(t_k\right)^T\cdot\mathbf{M}\cdot\mathbf{r}_j}{\boldsymbol{\varphi}_j\left(t_k\right)^T\cdot\mathbf{M}\cdot\boldsymbol{\varphi}_j\left(t_k\right)}=1 \quad (2)$$

Where $\alpha_{ij}\left(t_k\right)=$the ratio between the seismic load participation factor and the modal mass associated with the i-th mode shape and the j-th seismic input. Overall, the mass matrix and the mode shapes for all DOFs are commonly unknown for real-scale structures. Hence, $\alpha_{ij}\left(t_k\right)$ values need to be estimated or adjusted during the optimization process. $\boldsymbol{\psi}_i\left(t_k\right)=$the i-th not-normalized mode shape can be calculated from system identification techniques, computed from the eigenvalue problem of $\mathbf{M}^{-1}\cdot\mathbf{K}$ ($\mathbf{K}$ the stiffness matrix), or any other group of orthogonal mode shapes. For actual buildings, the mode shapes are 3D and include

longitudinal, transverse, and torsional responses and can be estimated from ambient vibration tests.

The usage of normalized mode shapes offers a convenient relationship that allows disaggregating the variation of mode shapes from effects of damping fluctuations (both parameters can modify the amplitude of the relative response), i.e., the optimization problem is also constrained to fulfill the following identities (for each seismic input),

$$\sum_{i=1}^{N} \boldsymbol{\varphi}_{ij}\left(t_k\right) = \mathbf{r}_j \Rightarrow \sum_{i=1}^{N_2} \boldsymbol{\varphi}_{ij}\left(t_k\right) = \sum_{i=1}^{N_2} \boldsymbol{\psi}_i\left(t_k\right) \cdot \alpha_{ij}\left(t_k\right) = \tilde{\mathbf{r}}_j \approx \sum_{i=1}^{N_2} \boldsymbol{\varphi}_{ij}\left(0\right) \;\; \forall j \tag{3}$$

Therefore, there is a group of normalized mode shapes for each j-th seismic input. They share the same root group of not-normalized mode shapes $\boldsymbol{\psi}_i\left(t_k\right)$ (which are time-variant during the optimization process) but $\alpha_{ij}\left(t_k\right)$ must be selected to fulfill Eq.(3) for each j-th seismic input, observing that $\boldsymbol{\varphi}_{ij}\left(0\right)$ refer to the normalized seismic mode shape at the initial time. Because normalized seismic mode shapes are employed, the time modal response ($Y_{ij}\left(t\right)$) is described by a nonlinear SDOF system subjected to the j-th acceleration ground motion ($\ddot{v}_g^j\left(t_k\right)$) as follows (observing that the modal SDOF response is described without any load participation factor),

$$\ddot{Y}_{ij}\left(t_k\right) + 2 \cdot \zeta_i\left(t_k\right) \cdot \omega_i\left(t_k\right) \cdot \dot{Y}_{ij}\left(t_k\right) + \omega_i^2\left(t_k\right) \cdot Y_{ij}\left(t_k\right) = -\ddot{v}_j^g\left(t_k\right) \tag{4}$$

The modal responses are computed for each i-th mode and each j-th seismic input according to a traditional constant acceleration numerical approach modified by Hernandez et al. [40,41] to account for time-variant dynamic properties. It is to be noted that $\zeta_i\left(t_k\right)$ and $\omega_i\left(t_k\right) = 2 \cdot \pi \cdot f_i\left(t_k\right)$ refers to the time-variant damping ratio and natural angular frequency associated with the i-th mode. $f_i\left(t_k\right)$ is the time-variant natural frequency related to the i-th structural mode response.

Overall the Mod-ζ(var) method solves an optimization problem where the modal parameters are adjusted by small data windows to minimize the difference between the model-predicted absolute acceleration response and the experimental data for all measured output channels (in the time and frequency domains). That is, $\zeta_i\left(t_k\right)$, $f_i\left(t_k\right)$, $\boldsymbol{\psi}_i\left(t_k\right)$ and $\alpha_{ij}\left(t_k\right)$ are time-variant modal parameters that are iteratively adjusted by assuming linear functions over small data windows [40,41]. Thus, the initial values of these modal parameters are consequently taken from the previous window. So, it ensures continuity of the modal and model-predicted responses, i.e., Eq.(1) and Eq.(4) become continuous functions. Similarly, the initial modal responses ($\dot{Y}_{ij}\left(t_k\right)$ and $Y_{ij}\left(t_k\right)$) are also directly obtained from the previous window. Accordingly, the final values for the modal parameters related to the analyzed data window are consequently optimized to minimize the difference between the model-predicted response

(Eq.(1)) and the experimental data (the recorded seismic outputs). Overall, the optimization process is performed in two steps. First, the final values of the natural frequencies and damping ratios associated with the analyzed data window are adjusted, considering that the normalized mode shapes remain constant and equal to the final values obtained from the previous window. As it were, these values are optimized to minimize the transfer function error (which should be equal to one for all frequencies), and the phase shift error (that should be zero for all frequencies) in the frequency domain between the model-predicted response and experimental data. Therefore, the first step is mainly focused on fitting the frequency content of signals. The normalized mode shape values (non-normalized mode shapes and $\alpha_{ij}(t_k)$ parameters) are then adjusted in the second step, considering the time-variant natural frequencies and damping ratios estimated during the first step. The NRMSE errors between the model-predicted responses and output signals are minimized in the time domain (i.e., the second step is focused on matching the signal amplitudes). It is important to note that each group of normalized mode shapes (for each j-th seismic input) is consequently constrained to fulfill Eq.(3), which is included in the objective error function [40,41]. As a result, the normalized mode shape offers a physical meaning, and variations of damping ratios are not misunderstood as fluctuation of normalized mode shape and vice versa (allowing disaggregate effects of damping ratios and mode shapes on the signals' amplitudes).

It should be pointed out that the initial modal parameters ($\zeta_i(0)$, $f_i(0)$, $\boldsymbol{\psi}_i(0)$ and $\alpha_{ij}(0)$ $\forall i \wedge \forall j$) should be pre-estimated before performing the Mod-ζ(var) approach. This process can be achieved according to the following procedure:

i) The initial structure's dynamic properties ($\zeta_i(0)$, $f_i(0)$, $\boldsymbol{\psi}_i(0)$) can be estimated from OMA (e.g., using the FDD method [44] and the procedure described in Appendix A) or from seismic data related to a minor seismic event (e.g., employing the DSI method [2]), meanwhile the structure behaves linear-elastic.

ii) The $\alpha_{ij}(0)$ can be pre-estimated from the estimated mode shape $\boldsymbol{\psi}(0)=\left[\boldsymbol{\psi}_1,...,\boldsymbol{\psi}_{N_m}\right]$ using the Moore-Penrose pseudoinverse, $\boldsymbol{\alpha}_j=\boldsymbol{\psi}^{\dagger}(0)\cdot\tilde{\mathbf{r}}_j$ (with $\boldsymbol{\alpha}_j=\left\{\alpha_{1j},...,\alpha_{N_m j}\right\}$).

iii) Using seismic data recorded from a minor seismic event, the $\alpha_{ij}(0)$ can be estimated again by minimizing the difference between the model-predicted response (Eq.(1)) and the recorded data, assuming constant natural frequencies and damping ratios estimated from a linear-elastic system identification technique such as the DSI method [2] (the initial values to be used during the optimization process can be obtained from step ii). As a result, $\boldsymbol{\varphi}_{ij}(0)=\alpha_{ij}(0)\cdot\boldsymbol{\psi}_i(0)$ can be estimated to carry out the Mod-ζ(var) approach.

It should be observed that the normalized mode shapes $\boldsymbol{\varphi}_{ij}(t_k)$ should have values between -0.5 to 1.5 times $\tilde{\mathbf{r}}_{ij}$ according to their physical meaning and the condition expressed in

Eq.(3). In this context, the global mode shape error described in [40] (shown in Figure 16 for the studied case) can be employed to indicate the error in estimating seismic normalized mode shapes. Figure 1 shows a general scheme of the Mod-ζ(var) approach used to identify 3D structures subjected to multiple seismic inputs.

Overall, the quality of the modal parameters' estimation can be evaluated by comparing the model-predicted response and experimental data for all output channels in the time and the frequency domains. The modal parameters related to a particular structural mode affect the seismic response for all output channels on a limited frequency. Therefore, a good agreement for all channels around the natural frequency of the analyzed mode suggest that the modal parameters were properly estimated. Differences between the model-predicted response and the seismic data will always occur because the noise contained into the signals (inputs and outputs), errors on the modal parameter estimation, local variations of modal parameters that cannot be accounted by the linear assumption by small data windows, etc. Overall, a complex nonlinear response is modelled as an equivalent nonlinear modal system.

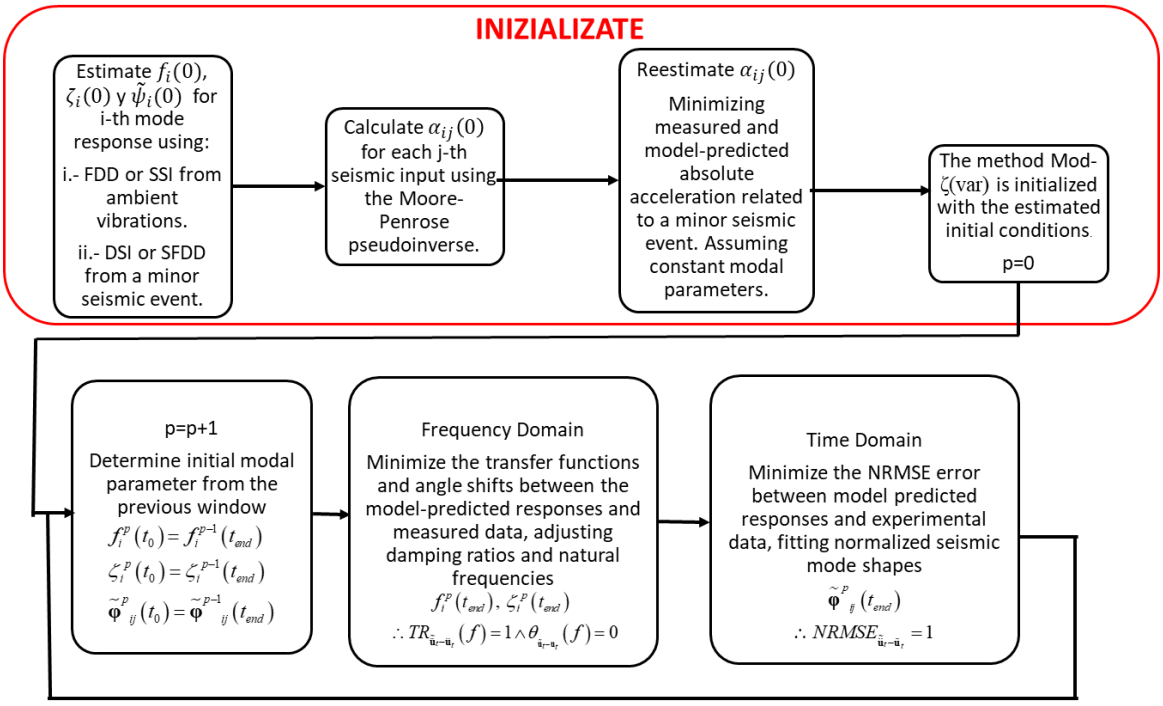

Figure 1: Scheme of the Mod-ζ(var) approach for 3D structures subjected to multiple seismic inputs

3. DESCRIPTION OF JUSTICIA ESPADA ACUÑA MENA (JEAM) BUILDING

The Justicia Espada Acuña Mena (JEAM) (ex-Central Tower, Figure 2) is a mid-height office building constructed in 1962 located in the center of the Faculty of Physic and Mathematics Sciences of the University of Chile in Santiago (Lat 33º27'27.59' 'S, Long 70º39'44.02"W). The building was renamed in 2021 to honor the first woman entitled to be a civil engineer at the University of Chile in 1919 [45]. The building's height is 30.2 meters, with eight stories, and two basements (Figure 3). It exhibits a general plan area of 31 meters by 19 meters along longitudinal and transverse directions (with a total surface of 4602 m^2). It corresponds to an

R/C shear wall building with wall thicknesses of 35 cm (i.e., the ratio between total wall area to plan is 7.7%) with slabs of 25 cm and complementary peripherical R/C frames conformed by beams and short columns. The building is founded over dense gravel 75-100 meters in depth up to the bedrock with an almost flat H/V Nakamura ratio (with a small H/V peak value related to an amplification factor of 2 associated with a site natural frequency of 0.6-0.8 Hz) and a shear wave velocity, V_{s30}, ranging from 550-600 m/s [46]. Since its construction, the building has experienced multiple structural and architectural modifications, but the most important ones were done before 2010 [42] (i.e., previous to the data processed in this article). For example, openings have been added to a few structural walls, distributions of nonstructural walls have been modified, and external steel frames have been added to achieve a more modern style, which adds mass to the structure and almost negligible stiffness. Figure 2 shows a general view of the building from different orientations.

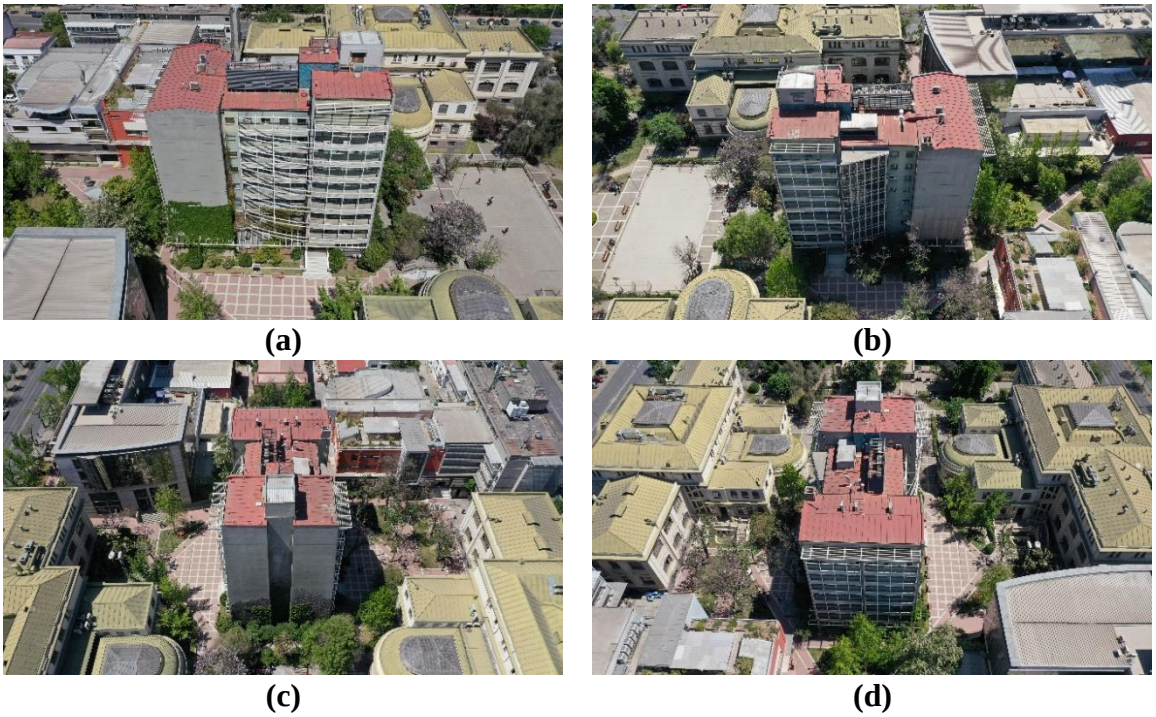

Figure 2: JEAM Building: (a) North view, (b) South view, (c) West View, (d) East View

The JEAM building was seismically instrumented in 2009 [47] by the National Net of Accelerograph (RENADIC) of the University of Chile. The net of seismic sensors corresponds to eight unbalanced uniaxial accelerometers EpiSensor ES-U2 from Kinemetrics set to measure ±0.25g and placed according to the layout distribution displayed in Figure 3. Two accelerometers are positioned on the base (to measure the longitudinal and transverse seismic inputs), and two arranges of three accelerometers are placed on the third and eighth floors of the building, respectively (two transverse and one longitudinal) to capture the longitudinal, transverse, and torsional responses. The net has two acquisition systems working in parallel, i.e., a DaqBook/200 16 bit-100kHz and a LogBook/360 16bit-100 kHz. The Daqbook/200 is focused on ambient vibration data (AVD) that are periodically recorded every 15 minutes (15-minute length) and are processed by a local PC connected to the system. The Daqbook/200 includes two DBK 18 Lotech cards to amplify the AVD by a gain factor

of 10. The LogBook/360 acquisition system is configurated without amplification to record intermediate seismic events. The seismic data is stored when the base acceleration traces exceed a threshold of 0.01g. Both acquisition systems record data to a sampling frequency of 200 sps. The DaqBook/200 also records the soil saturation at different levels under the ground (3 sensors placed at 20, 10, and 5 meters below the ground surface), located inside a covered well beside the west edge of the building.

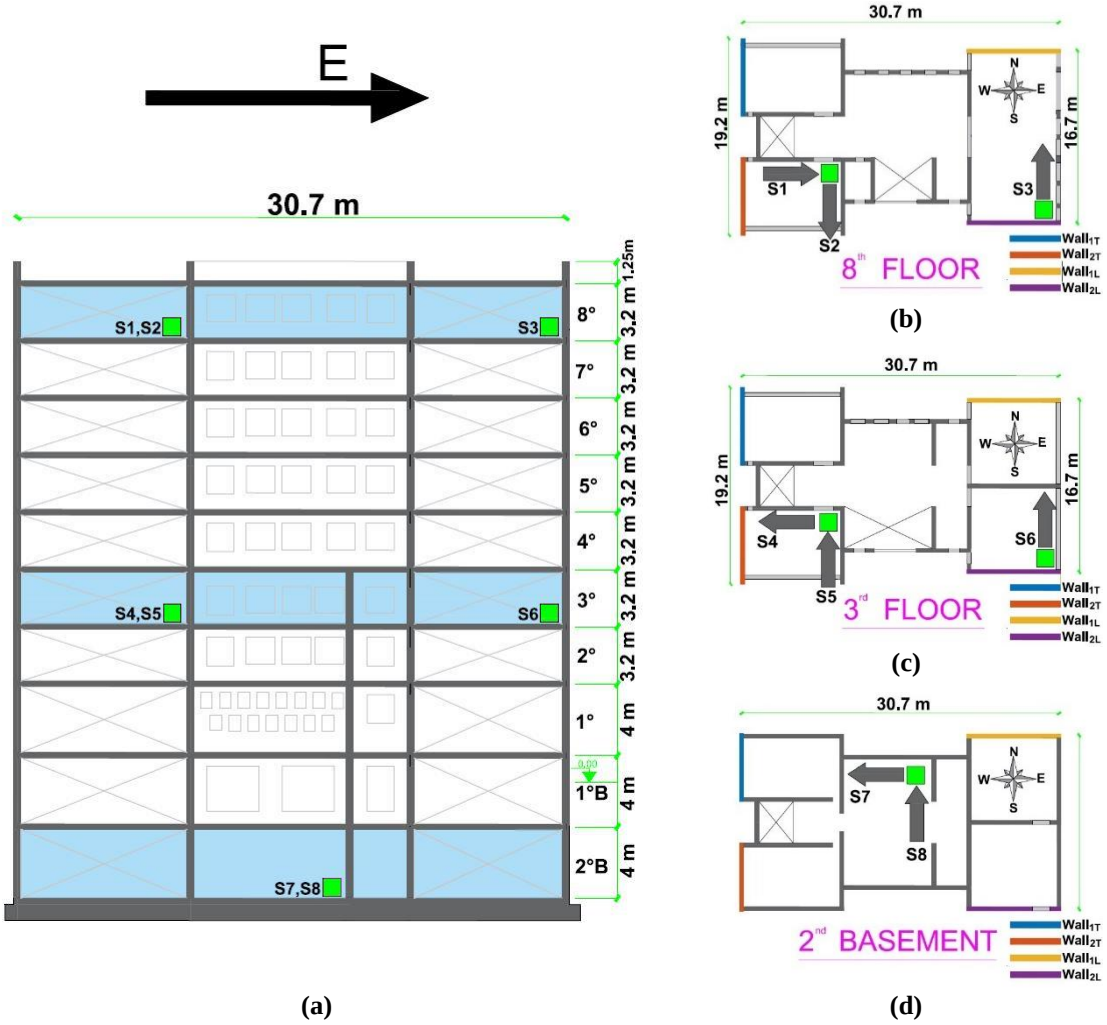

Figure 3: (a) Accelerometers locations, elevation view along the longitudinal direction, (b) sensors installed on the 8th story, (c) accelerometers installed on the 3rd story, (d) sensors installed on the 2nd basement

Based on this instrumentation, a Structural Health Monitoring (SHM) network was implemented for the JEAM building based on OMA, where real-time results were continuously published on an SHM website allocated for the JEAM building [48–50] (updating results every 15 minutes). The JEAM-SHM website published in real-time identified natural frequencies, damping ratios, and mode shapes computed with the SSI [2] and PSD [51] methods. The SHM network was also connected in real-time with a meteorological station maintained by the Meteorology Group of the Geophysics Department at the University of Chile, which is installed over the roof of a neighboring building 40 meters distance. Therefore, the SHM system also recorded several environmental parameters such

as temperature, rainfall, wind speed, relative humidity, and air pressure. Further details about the instrumentation can be reviewed in [52]. The SHM network observed that the natural frequencies obtained from OMA had experienced variation due to environmental conditions, i.e., 4% frequency changes related to temperature fluctuations and 6% because of rainfall and humidity variations [49,50].

Table 1 shows the natural frequencies that were determined using OMA just before (02/26/2010) and just after (03/03/2010) the central Chilean mega-earthquake Mw=8.8 (02/27/2010) [42,48–50,52]. AV data before and after the earthquake was recorded using the permanent seismic instrumentation displayed in Figure 3 and collected by the SHM monitoring network. From Table 1, it can be observed that the natural frequencies of the JEAM building experienced a sudden and permanent decrease (between 3.6-19.1%) of its natural frequencies because of the 02/27/2010 mega-earthquake Mw=8.8, which was associated with minor cracks observed on shear walls and nonstructural components [42]. It should be noted that these reductions were clearly observed from the results displayed by the SHM network, where natural frequencies experienced a sudden jump after the earthquake [42]. Similar variations before and after the mega-earthquake were also observed for the vertical wave velocity estimated by Rahmani et al. [53] from interferometry techniques.

Table 1: Natural Frequencies from OMA and FEM, before and after the 2010 earthquake

	Before Earthquake 02/26/2010	**After-Earthquake 03/03/2010**		**After-Earthquake* 11/25/2021**	**Idealistic uncracked ETABS FEM**	
Mode**	Frequency (Hz)	Frequency (Hz)	Difference (%)	Frequency (Hz)	Mode	Frequency (Hz)
1-Tr-To	2.25	1.89	19.05	1.90	1-Tr-To	2.46
2-Lo	2.62	2.30	13.91	2.37	2-Lo	3.72
3-Tr-To	2.98	2.67	11.61	2.77	3-To-Lo-Tr	4.35
4-Tr-To	6.30	5.46	15.38	5.61	4-Tr	9.08
5-Lo	7.47	6.68	11.83	6.77	5-Lo	13.02
6-Tr-To	8.18	7.50	9.07	7.58	6-To	15.53
7-Tr-To	9.26	8.31	11.43	8.41	7-Tr-To	18.76
8-Lo	10.62	10.25	3.61	10.07	8-Lo	25.79

* Estimated from a campaign of AV tests realized on 11/25/2021 detailed in section 4

**Tr=Transverse, To=Torsional, Lo=Longitudinal. Mode shapes 2nd, 5th, and 8th are longitudinal predominant. Other modes (1st,3rd,4th,6th,7th) refer to coupled transverse-torsional responses (Figure 5)

The natural frequency reductions are consistent with the dynamic properties estimated from a MIMO technique applied to small seismic events recorded before and after the central Chilean mega-earthquake Mw=8.8 [48]. Despite the significant variations in natural frequencies during the 2010 earthquake, the mode shapes have not evidenced relevant variations [42]. Figure 4 shows high Modal Assurance Criterion (MAC) values [54] computed from mode shapes pre and post-the Chilean mega-earthquake in 2010 (Mw=8.8). It should be pointed out that Table 1 also indicates the natural frequencies determined from a Finite Element Model (without a calibration process) of the JEAM building addressed in the commercial software ETABS [55] (which is employed for

validation of the Mod-ζ(var) approach in section 5). As a final observation, the SHM network has not evidenced perceptible variations of the dynamic properties of the JEAM building related to the three principal structural modes after the mega-earthquake in 2010.

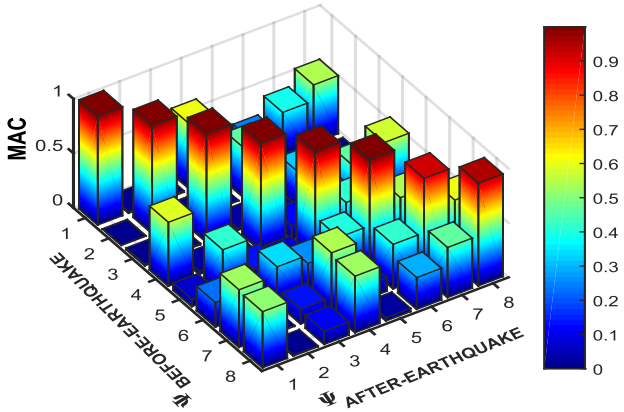

Figure 4: MAC values computed from modal shapes estimated from OMA after and before the earthquake

4. DYNAMIC PROPERTIES OF THE JEAM BUILDING FROM OPERATIONAL MODAL ANALYSIS (OMA)

Figure 5 shows a full 3D graphical representation of the structural mode shapes of the JEAM building that was estimated from Operational Modal Analysis (OMA). A campaign of six ambient vibration tests (AV) was performed on the JEAM building on 11/25/2021. A full 3D representation of the mode shapes of the JEAM building is helpful to visualize the building behavior for all its floors. However, even more relevant results can be employed to estimate global and local responses of the JEAM building (in section 7). In other words, the 3D mode shapes of the entire structure can be combined with nonlinear modal responses computed by the Mod-ζ(var) approach (in section 6) to estimate the local and global responses of the JEAM building, including unmeasured floors.

A campaign of six ambient vibration tests (AV) was performed on the JEAM building on 11/25/2021. The campaign was achieved by employing temporary instrumentation consisting of eleven uniaxial accelerometers Episensors ES-U2 from Kinemetrics set to a threshold of ±0.5g, an acquisition system DaqBook/2000 (16 bits-200 kHz and 16 terminals, with a gain factor of 10) and a laptop with DaqView software. The reduced number of available sensors prompted six AV tests to measure all floors of the JEAM building. Overall, three accelerometers were installed on the eighth floor (Figure 2); two transverse and one longitudinal oriented and placed far from the geometrical center to measure the floor's longitudinal, transverse, and torsional responses. The three sensors were kept in the same position for all AV tests; thus, they were employed to measure the reference floor. Similarly, two sensors were held on the building base during all AV tests. Six accelerometers were sequentially installed on two different floors during each AV test, i.e., requiring four AV tests to measure nine floors of the building, excluding the roof. Two sensors were installed along the transverse direction and one along the longitudinal direction, allowing the recording

of the other two floors' transverse, longitudinal, and torsional responses during AV tests. AV tests were performed for 40 minutes, and a sampling frequency of 200 sps was employed.

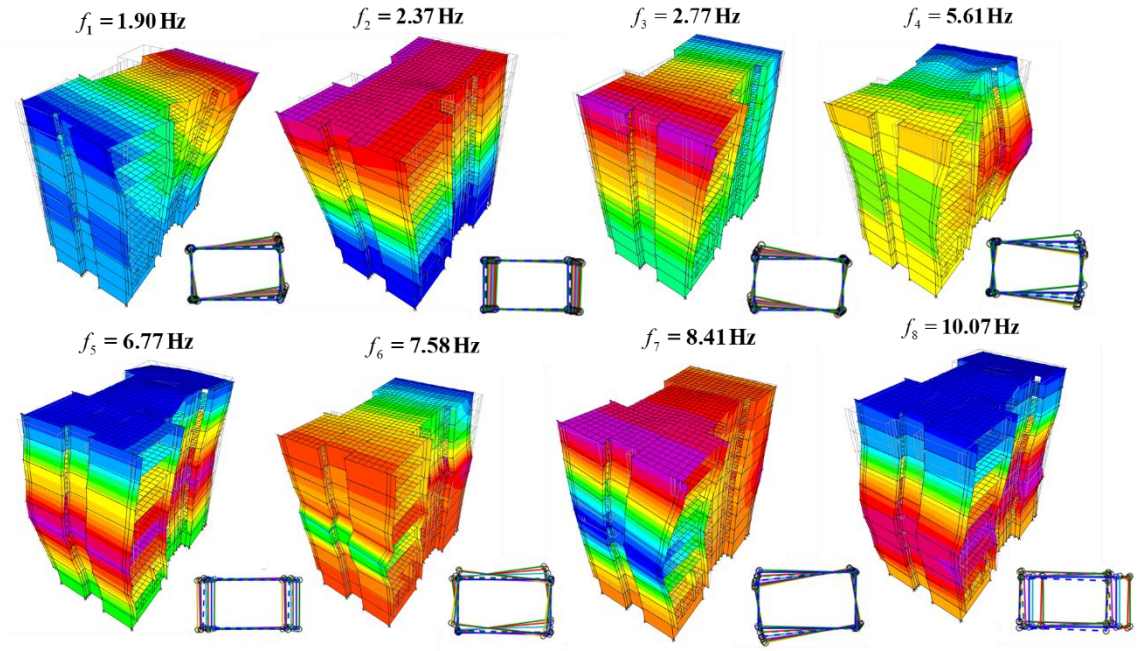

Figure 5: Mode shapes and natural frequencies estimated from OMA performed on 11/25/2021. The color scale of 2nd, 5th, and 8th is related to longitudinal movement. The color scale of 1st, 3rd, 4th, 6th, and 7th is related to transverse movement. Red refers to the maximum value, and blue is the minimum value.

The AV data related to AV tests were processed using SSI [2] and FDD [44] system identification techniques. Figure 6a displays the stabilization diagram obtained from the SSI-Data method (with UPC weighting flag) related to the first AV test. Similitude criteria of 5 % for frequency, 5 % for damping ratios, and 10 % for MAC [54] were employed to generate the Stabilization Diagram by considering a model order between 2 and 240. Figure 6a also shows the histogram of frequency coincidences and the average PSD obtained from all channels. Figure 6c presents the semi-log plot of the singular values obtained from the FDD method, using a Hanning window of 30 s in length and overlapped 15 sec with a frequency resolution of 0.01 Hz. Figure 6b exhibits the MAC values that compare the mode shapes estimated from SSI and FDD methods. Both system identification techniques show similar results, validating that an accurate estimation of the dynamic properties is obtained. In addition, the FDD method estimates a structural mode that cannot be easily identified from SSI (6th structural mode). Figure 5 shows the mode shapes and natural frequencies estimated by merging estimations made from ambient vibration tests using a multi-setup approach [56,57]. It was implemented by computing the mode shapes related to the geometrical center of each floor measured for each AV test, using a geometrical transformation and assuming rigid diaphragms for all the building floors. Then, mode shapes were scaled to match the movement of the referential floor associated with each independent structural mode and measurement, i.e., the mode shapes were scaled to minimize the distance between the four corners of the eighth floor.

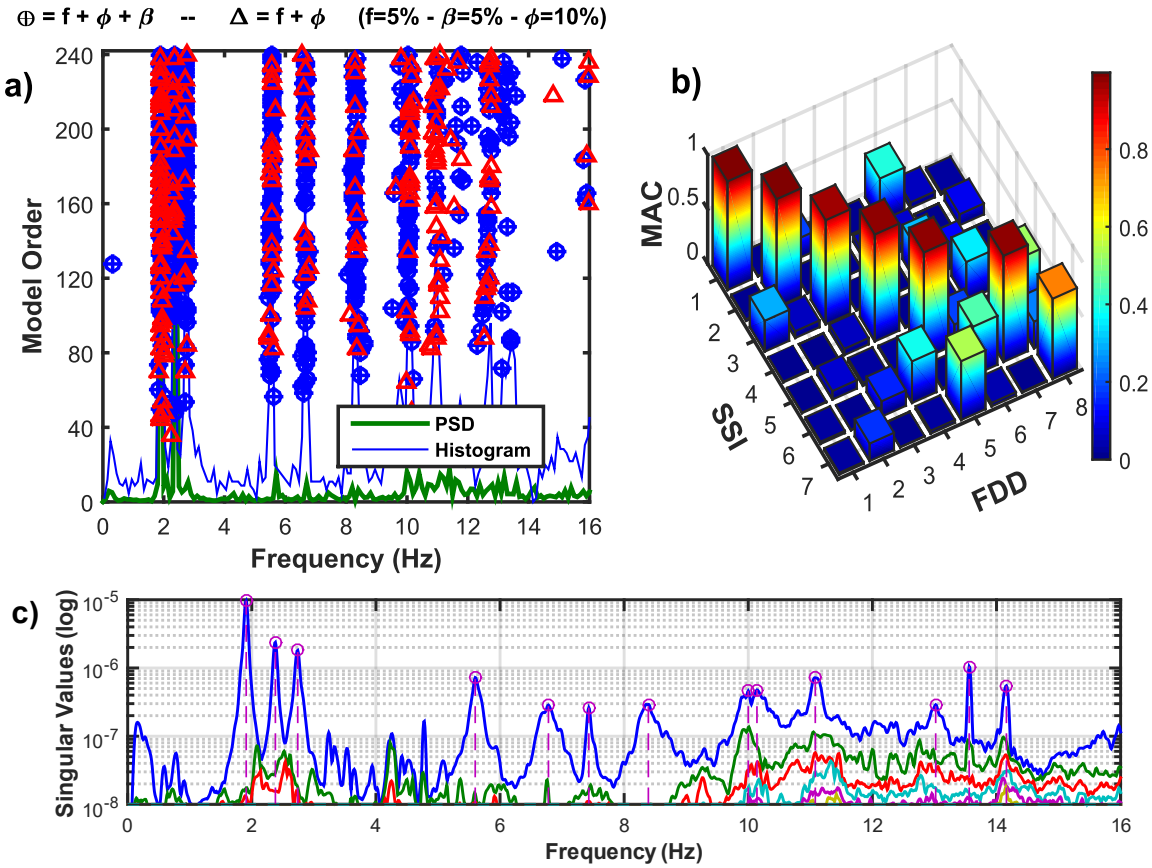

Figure 6: a) Stabilization Diagram from SSI [2], b) MAC comparison between SSI and FDD methods, c) Singular log-values of FDD [44] method related to AV test No.1

OMA results show that the natural frequencies estimated in November 2021 (Figure 5) are similar to the dynamic properties estimated in March 2010 based on the permanent seismic instrumentation, i.e., just after the 2010 mega-earthquake Mw=8.8 (Table 1). Notably, the differences in natural frequencies are in the range explained because of changes in environmental conditions. From the results, it can be concluded that the JEAM building has not experienced relevant structural variations since the mega-earthquake. It should be noted that the JEAM building has been subjected to multiple intermediate and small seismic events after 2010 (PGA<0.05g). It can be observed that the 2nd, 5th, and 8th mode shapes are mainly related to longitudinal movements with negligible torsional contributions. These results can be expected considering the symmetry of longitudinal walls observed in the plan distribution displayed in Figure 2. In contrast, the 1st, 3rd, 4th, 6th, and 7th mode shapes exhibited coupled transverse and torsional movements. In particular, the 1st and 4th structural modes are related to the building's transverse movement of its east flange. Similarly, the 3rd and 7th structural modes involved the response of the west flange of the JEAM building.

It can be observed that the top stories motions are mainly described by low-frequency structural modes (1st, 2nd, and 3rd), as shown in Figure 5. In contrast, bottom stories are controlled by low and high-frequency structural modes. In addition, the OMA mode shapes showed that the building's base level did not experience appreciable movements compared to the upper floors. It implies that mode shapes identified from OMA can be understood as

relative movements to the base level and can be employed for seismic analysis. Notably, sensors at the base level do not show significant energy for low frequency (<5 Hz) during AV tests.

5. VALIDATION OF MOD-ζ(VAR) METHOD FROM SIMULATED DATA USING A 3D LINEAR MODEL OF THE JEAM BUILDING

An idealistic Finite Element Model (FEM) of the JEAM building was developed using the commercial software ETABS [55], following the current seismic analysis practices in Chile. The FEM assumes a linear elastic behavior for the structure and considers an uncracked modulus of elasticity for concrete equal to 23750 MPa (concrete H30, according to the Chilean standard). However, the natural frequencies obtained from the FEM (Table 1) differ significantly from the natural frequencies identified through Operational Modal Analysis (OMA) before and after the mega-earthquake. It occurred because several aspects of the structure were not modeled, such as the soil-foundation-structure-interaction, interaction with nonstructural elements, the inclusion of external steel frames, unsymmetrical mass distributions, stiffness degradation due to structural damage, heterogeneity of materials, construction errors, or even structural deterioration occurred during the time. As a result, the seismic response obtained from the FEM may not match the actual response measured by sensors. It is important to note that the FEM does not need to be fine-tuned to match the dynamic properties of the OMA results. This is because the idealistic FEM is used as a study case to validate the Mod-ζ(var) approach. Furthermore, the idealistic FEM can be used to compare the results obtained from the current seismic analysis practices in Chile with the actual seismic response obtained from the Mod-ζ(var) approach (in section 7).

The FEM considers R/C shear walls and peripherical R/C frames modeled as linear shell and frame members, respectively. An additional seismic weight of 500 N/m^2 was uniformly distributed over all the building's floors. Other finishing-related seismic weights were also included as seismic masses distributed on the structural members. The small wall openings were not modeled by simplicity, and the external steel frames were not included, giving that the response is controlled by the large RC walls. The structure was assumed to be fixed on its base (i.e., under the 2^{nd} basement floor). Then, a modal time history analysis was performed considering the longitudinal and transverse seismic inputs recorded during the 2010 Chilean mega-earthquake (Mw=8.8). For simplicity, damping ratios were assumed to be constant and equal to 5% for all structural modes. Later, the absolute acceleration traces at the seismic sensors' position (Figure 3) were computed and extracted from the FEM. The idea was to generate a study case that can be employed to validate the Mod-ζ(var) approach. Then, the simulated data were treated as recorded seismic data that will be processed with the Mod-ζ(var) approach.

The simulated seismic data related to the sensor positions were assumed to be the recorded data (without adding noise). The simulated data was filtered with a Butterworth low-pass N=8 filter with a cutting frequency of 30 Hz before processing. This data was then processed with the Mod-ζ(var) approach, considering the first nine structural modes. The natural frequencies, damping ratios, and seismic normalized mode shapes that are employed as initial

parameters in the Mod-ζ(var) approach were directly extracted from the software. It is noted that normalized mode shapes at the sensor positions are determined from the mode shapes (obtained from a modal analysis) and their corresponding modal masses and load participation factors (reported by the software) associated with each direction of analysis.

Figure 7 shows the Mod-ζ(var) approach results applied to the simulated data. Figure 7a compares the model-predicted response obtained with the Mod-ζ(var) approach with simulated seismic data at the sensors' positions of the permanent seismic instrumentation allocated into the structure (Figure 3). Plots show a zoom window between 10 and 15 seconds to improve visualization of the comparison. Generally, the model-predicted response almost perfectly matches the simulated seismic data, considering that the lowest NRMSE value is 0.98 (1.00 implies perfect matching). Differences can be associated with numerical errors related to the numerical solution and the Mod-ζ(var) approach. Figure 7b shows the time-variant damping ratios estimated by the Mod-ζ(var) approach, compared with the damping ratios assigned for structural modes in ETABS. It can be observed that the Mod-ζ(var) approach estimated a constant 5% damping ratio for all structural modes and during the seismic record. Therefore, these results were identical to the values assigned to the FEM analysis. It should be pointed out that the 8th mode showed slight differences compared to analytical results that can be associated with numerical errors and effects of the low-pass filter that was previously applied to data before performing the Mod-ζ(var) methodology.

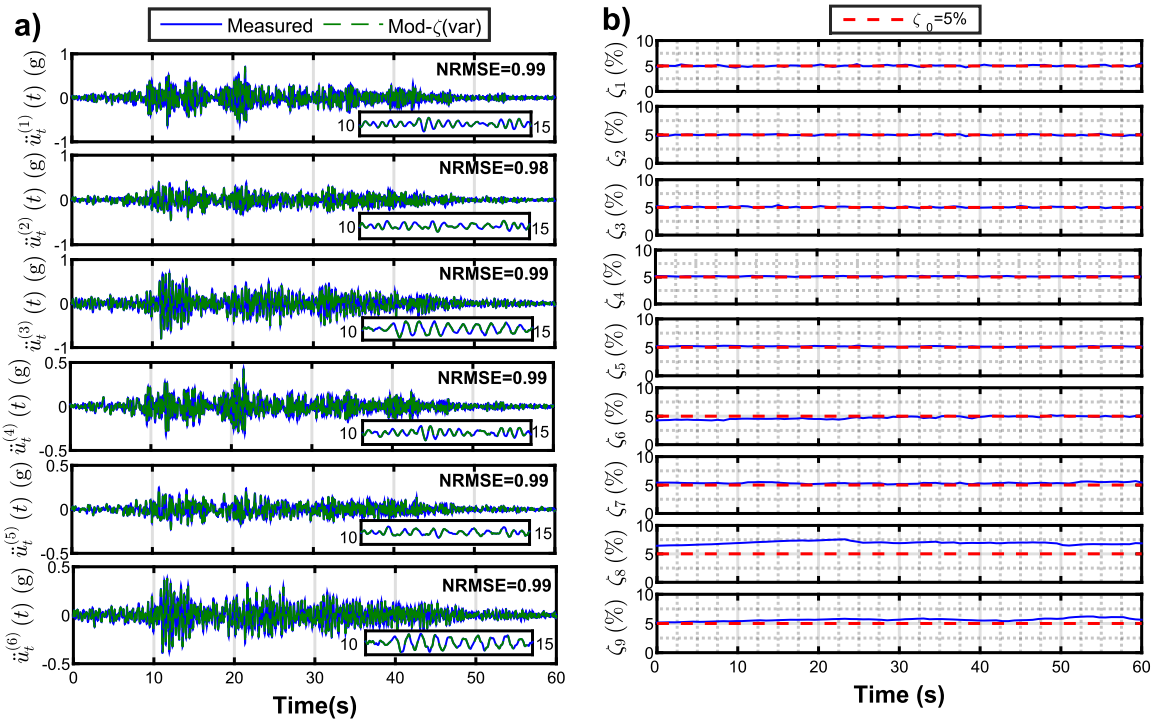

Figure 7: a) predicted model-response (Mod-ζ(var) approach) v/s seismic data related to sensor positions (S1, S2, S3, S4, S5, and S6) displayed in Figure 3 (from ETABS), b) Time-variant damping ratios estimation using the Mod-ζ(var) approach from ETABS simulated data

Figure 8a shows the time-variant frequencies (in color lines) obtained from the Mod-ζ(var) approach. The time-variant frequencies are plotted over the STTF [17], which were

calculated between the output signal computed on the 8th floor for the longitudinal direction (S1 of Figure 3) and the longitudinal seismic input (S7 of Figure 3). The STTF plots were computed using a Hanning window of 5 sec. Figure 8b shows similar results but related to the transverse direction, i.e., STTF was computed between the output signal S2 and the seismic input S8 (Figure 3). It can be observed that the natural frequencies are invariant over time and coincident with analytical values (detailed in Table 1).

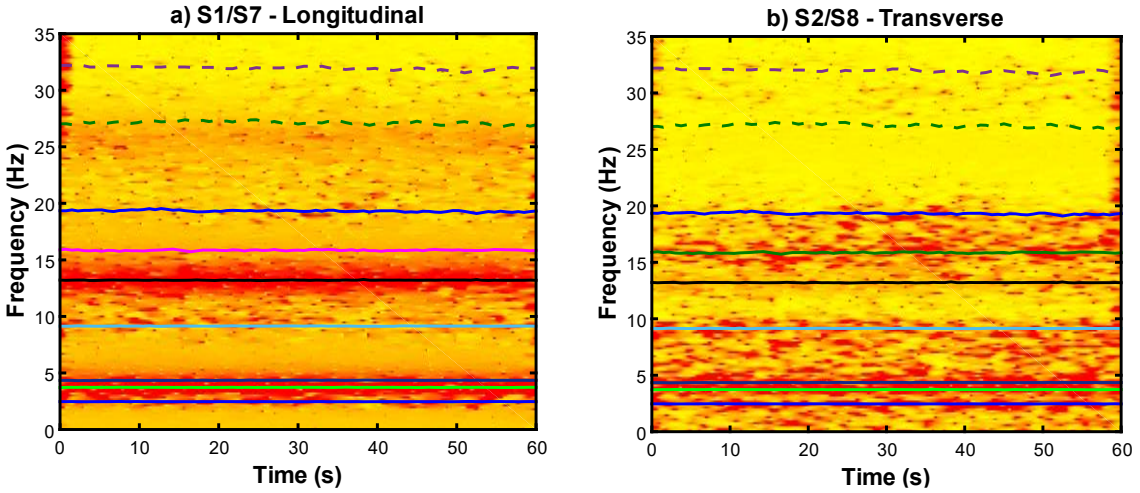

Figure 8: a) time-variant natural frequencies and STTF related to S1/S7 (longitudinal), b) time-variant natural frequencies and STTF related to S2/S8 (transverse) ETABS simulated data

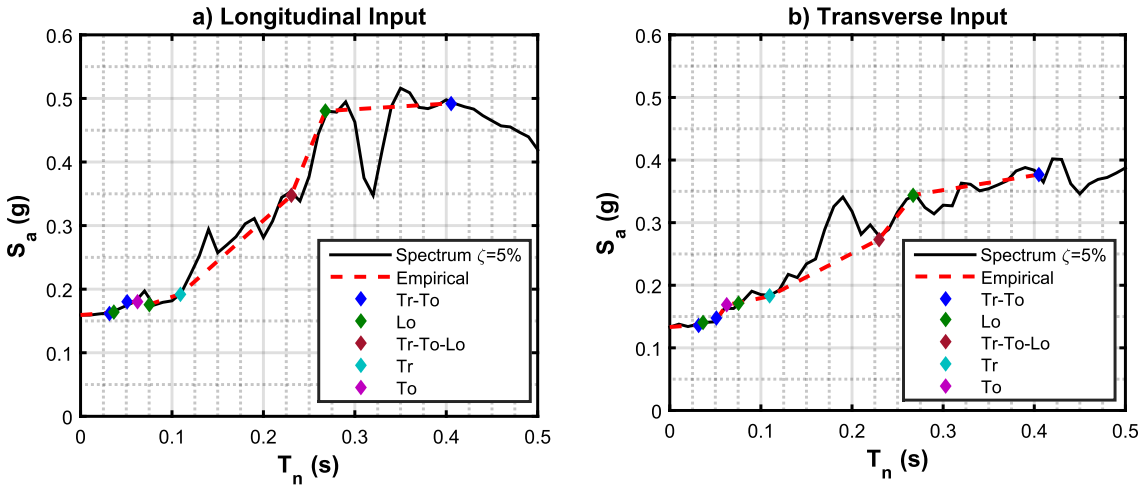

Figure 9:a) Empirical response spectrum (Mod-ζ(var) approach) and response spectrum related to the seismic input applied to the longitudinal direction, d) Empirical response spectrum (Mod-ζ(var) approach) and response spectrum associated with the transverse direction

Figure 9 shows the empirical response spectra obtained using the Mod-ζ(var) approach. Details about its computation are not described in this section, considering that section 7 shows details about this computation for the actual seismic case. Results are presented as discrete values connected with straight lines. Spectral values were computed from the peak absolute acceleration response of each mode obtained for the longitudinal and transverse seismic inputs. It is worth noting that the empirical response spectra can only be computed for the structure's natural frequencies. The term "empirical" is employed since they are

obtained from the Mod-ζ(var), which utilizes the seismic data (in this case, obtained from the FEM simulated data) to perform an inverse problem. Figure 9 also shows the response spectra computed from seismic inputs using a damping ratio of 5%. It is observed that the estimated results matched well with the spectra of the seismic inputs.

6. TIME-VARIANT DYNAMIC PROPERTIES AND EMPIRICAL RESPONSE SPECTRUM OF THE JEAM BUILDING DURING THE 2010 CENTRAL CHILEAN MEGA-EARTHQUAKE (MW=8.8).

Estimating the initial modal parameters is required before carrying out the Mod-ζ(var) approach. These initial modal parameters were determined from processing the seismic data of a minor seismic event recorded just before the 2010 central Chilean mega-earthquake (Mw=8.8). The DSI [2] and SFDD [39] methods were employed to estimate the dynamic properties related to a seismic event recorded on 02/12/2010 (15 days before the mega-earthquake, an event with Mw=6.2). It was expected that the JEAM building would exhibit an almost linear-elastic seismic response. The base acceleration records (sensors S7 and S8 in Figure 3) were the seismic inputs, and the rest of the channels (S1 to S6) were the outputs. Figure 10a shows the stabilization diagram obtained with the DSI method assuming a model order between 2 to 100 and using similitude criteria of 1% for natural frequencies, 7% for damping ratios, and 10% for mode shapes (including average PSD of output channels and the frequency histogram). Figure 10b shows the semi-log plot of singular values obtained from the SFDD method using the longitudinal and transverse seismic inputs (using a Hanning window of 7.0s in length overlapped 3.5s with a frequency resolution of 0.01 Hz).

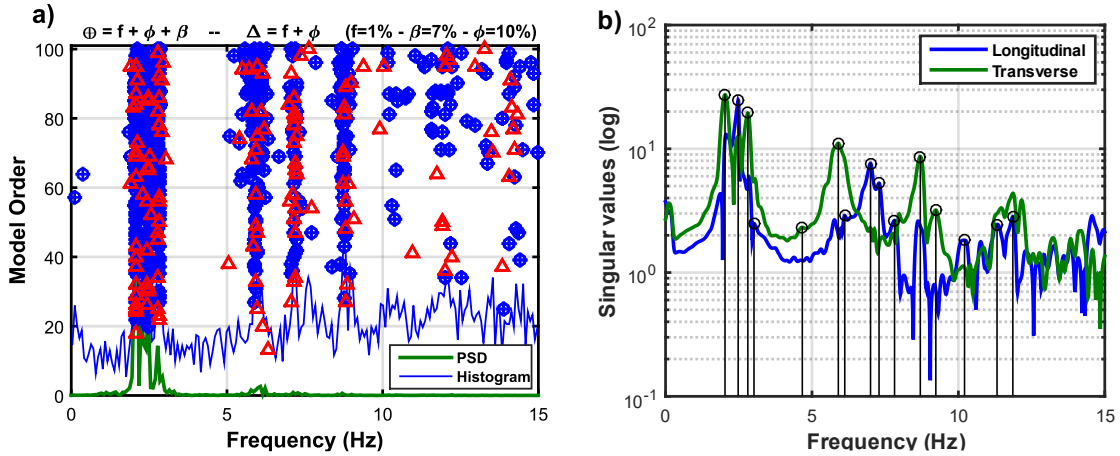

Figure 10: a) Stabilization diagram determined with DSI method b) log-singular values of SFDD method applied to a minor seismic event that occurred on 02/12/2010 Mw=6.2 (before the mega-earthquake)

Table 2 shows natural frequencies and damping ratios identified from the minor seismic event before the mega-earthquake (02/12/2010 Mw=6.2). Overall, seven structural modes (1st, 2nd, 3rd, 5th, 6th, 8th, and 10th) are identified from both system identification techniques (DSI and SFDD). The SFDD allows for identifying structural modes that are not recognized using the DSI method but are secondaries in the seismic response. Similarly, Table 3 shows the same results but related to data of a low-intensity seismic event that occurred after the mega-

earthquake (03/11/2010 Mw=6.3, 12 days after). Table 2 and Table 3 show damping ratios estimated from DSI method; other structural modes identified only with SFDD assume an initial damping ratio of 1% (they will be later adjusted by the Mod-ζ(var) approach). The comparison between mode shapes estimated before and after the earthquake shows that they do not exhibit significant variations. In this context, Table 3 shows a plan view of the mode shapes related to measured floors (the 8th floor in green, the 3rd floor in red, and the fixed base in blue) estimated from data before and after the earthquake. It can be observed that the 4th mode seems to be an artificial mode caused by the vibration of an object near sensor S1 (however, it does not contribute significantly to the seismic response).

Table 2: Natural Frequencies and damping ratios from DSI and SFDD methods related to a seismic event that occurred on 02/12/2010 Mw=6.2 (before the mega-earthquake)

Mode	**1st**	**2nd**	**3rd**	**4th**	**5th**	**6th**	**7th**	**8th**	**9th**	**10th**	**11th**
Type	**Tr-To**	**Lo**	**Tr-To**	Lo	Tr	**Tr-To**	Lo-To	**Lo**	**Lo-To**	Tr-To	**Lo-Tr**
$f_i(Hz)$	2.03	2.48	2.81	3.02	4.67	5.90	6.12	7.00	7.82	8.70	10.21
$\zeta_i(\%)$	1.93	2.16	1.88	1.00	1.00	2.88	2.48	1.85	1.00	1.19	1.00

Table 3: Natural Frequencies and damping ratios from DSI and SFDD methods related to a seismic event that occurred on 03/11/2010 Mw=6.3 (after the mega-earthquake)

$f_i(Hz)$	1.59	1.85	2.45	2.76	3.74	4.58	5.01	5.75	6.31	7.34	8.54
$\zeta_i(\%)$	4.81	3.49	3.38	3.92	1.00	4.71	1.00	1.00	1.00	1.00	1.00
OMA	**1**	**2**	**3**	**-**	**-**	**4**	**-**	**5**	**6**	**7**	**8**
	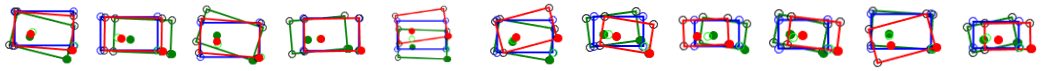										

It should be observed that the natural frequencies identified from seismic data (Table 2 and Table 3) are smaller than those determined from OMA (Table 1). These differences occur even for small seismic motions because the building experiences a fast reduction of natural frequencies at the beginning of the seismic motion (PGA<0.003g). For example, Figure 11 shows the STTF (computed with a Hanning window of 10 sec) related to sensors S1/S7 (Longitudinal) and S2/S8 (Transverse) associated with minor seismic events recorded before and after the mega-earthquake. It can be observed that the initial and final natural frequency values are similar to the determined from OMA (Table 1). However, they are rapidly reduced during the strong phase of the ground motion to values equal to the identified by using traditional seismic system identification techniques (displayed in Table 2 and Table 3). For example, Figure 11a shows that the natural frequency related to the second structural mode at the beginning and the end of the seismic event (before the mega-earthquake) is 2.58 Hz, which is similar to the 2.62 Hz obtained from OMA in Table 1. However, the natural frequency related to the second structural mode experiences a sudden reduction to a value of 2.48 Hz during the strong seismic motion, which is consistent with the natural frequency estimated from the DSI system identification technique (Table 2).

To sum up, the natural frequencies identified from OMA are higher than those computed from seismic data because the building experiences an almost immediate stiffness degradation that could be hypothetically related to previous residual damage. In other words, the fast reduction of stiffness could be explained by the presence of micro-cracks in the structural walls that are rapidly reopened at the beginning of the seismic motion. Similarly,

the natural frequencies are recovered (for small seismic events) at the end of the seismic event because micro-cracks are closed because of the self-weight of the building. The JEAM building has been subjected to multiple seismic events during its lifespan. For example, it was subjected to the central Chilean earthquake (Mw=7.8) in 1985, i.e., before installing the seismic instrumentation, which could have generated slight structural damage and might explain the fast frequency reduction observed before the 2010 Chilean mega-earthquake.

Figure 11 confirms that the same mode responses describe the structural movements for AV tests and seismic loading; however, they are characterized by different natural frequencies because they are quickly reduced during seismic motions. As a result, Table 3 shows the OMA's mode shapes of the entire building estimated from AV tests that can be associated with the mode shapes computed from seismic analyses. It should be pointed out that this assumption is valid because mode shapes do not exhibit significant variations during the seismic events and also because mode shapes estimated from AV data (Figure 5) are relative to the base level. That is, the base floor does not show significant movement during AV tests. Therefore, it is not required to transform the OMA dynamic properties to the seismic ones. Similarly, the seismic records measured by sensors installed on the base level are not described by the natural frequencies of the JEAM building during a seismic event, i.e., the earthquake source and the site response define their frequency content.

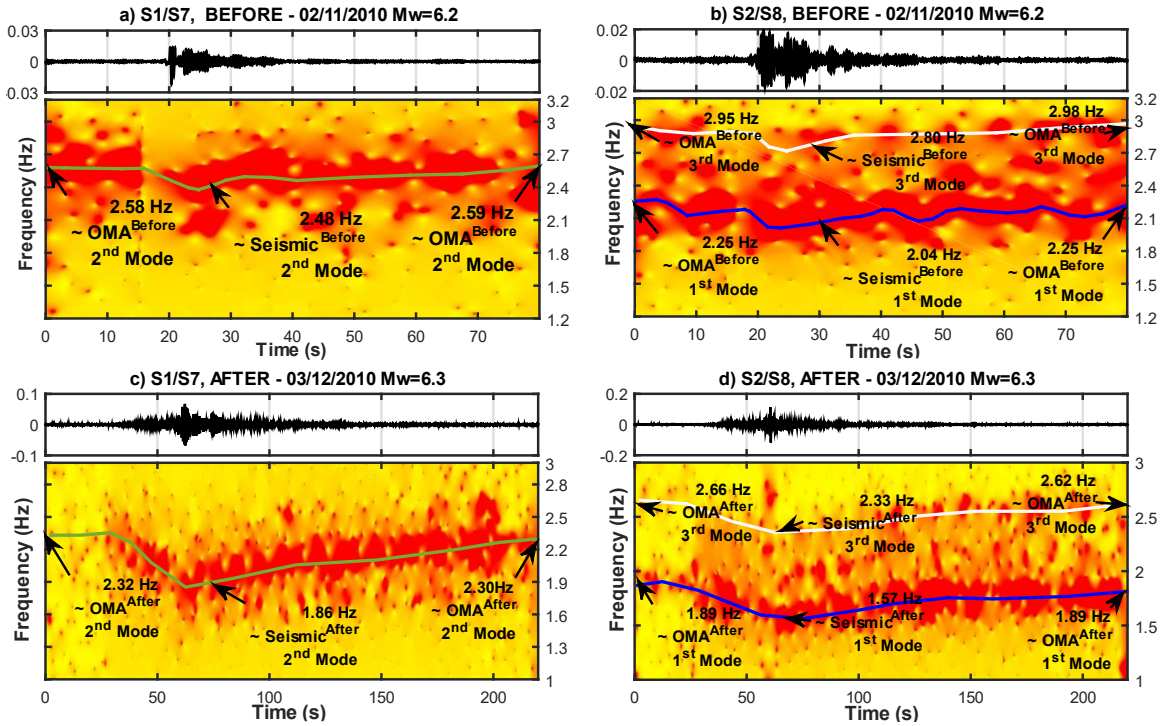

Figure 11: STTF and natural frequencies related to a) S1/S7 (longitudinal) seismic event before mega-earthquake 02/11/2010 (2nd mode), b) S2/S8 (transverse) seismic event before mega-earthquake 02/11/2010 (1st and 3rd modes), c) S1/S7 (longitudinal) seismic event after mega-earthquake 03/12/2010 (2nd mode), d) S2/S8 (transverse) seismic event after mega-earthquake 03/12/2010 (1st and 3rd modes)

Once the dynamic properties of the JEAM building are estimated at the sensors' positions, the seismic normalized mode shapes can be obtained following the procedure described in

section 2. The theoretical influence seismic vectors ($\tilde{\mathbf{r}}_j^{(theoric)}$) are defined according to the direction and orientation of sensors described in Figure 3. Then, the seismic response related to the minor seismic event (02/12/2010 Mw=6.2) is computed using constant dynamic properties described in Table 2, and $\alpha_{ij}(0)$ parameters are determined to minimize differences with seismic data. Finally, the initial seismic normalized mode shapes ($\boldsymbol{\varphi}_{ij}(0) = \alpha_{ij}(0) \cdot \boldsymbol{\psi}_i(0)$) and the initial influence seismic vectors ($\tilde{\mathbf{r}}_j$ in Table 4) are obtained. It can be observed that the initial seismic influence vectors are similar to the theoretical values. Differences could be explained because of a not-perfect orientation of sensors (e.g., S4 is not perfectly aligned with S7), errors in estimating mode shapes, and the lack of normalized mode shapes of higher natural frequencies.

Table 4: Influence seismic vectors, theoretical, initial, and corrected

	Direction	**S1**	**S2**	**S3**	**S4**	**S5**	**S6**
$\tilde{\mathbf{r}}_j^{(theoric)}$	Longitudinal	-1	0	0	1	0	0
	Transverse	0	-1	1	0	1	1
$\tilde{\mathbf{r}}_j \approx \sum_{i=1}^{N_2} \boldsymbol{\varphi}_{ij}(0)$	Longitudinal	-1.252	-0.125	-0.054	1.041	-0.244	-0.047
	Transverse	0.066	-1.104	0.721	-0.074	0.468	0.973

Based on the initial dynamic properties estimated from the minor seismic event, the Mod-ζ(var) approach is then applied to the seismic data recorded during the Chilean mega-earthquake (using a window length $t_{window} = 0.96\,s$, similar to the double of the first natural period, and a time between consecutive intercalated windows $\Delta t_{window} = 0.06\,s$ [40]). Figure 12 shows the absolute acceleration adjusted with the Mod-ζ(var) approach compared with the original seismic data related to the 02/27/2010 central Chilean mega-earthquake (Mw=8.8). A reasonable adjustment can be observed, considering that the NRMSE values are higher than 0.63 for the output channels employed for the adjustment process. Sensors on the eighth floor (S1 and S2) were accurately adjusted (NRMSE≥0.82), because they were mainly described by low-frequency structural modes (1st, 2nd, and 3rd structural modes of Table 3). In contrast, acceleration traces related to the third floor (S4, S5, and S6) show an inferior fit, which is explained because they are more sensitive to higher frequency structural modes. It should be observed that Figure 12 shows a time zoom between 20 and 30 seconds to improve visualization of the comparison during the strong motion phase.

It is emphasized that sensor S3 was not considered valid for the Mod-ζ(var) adjustment because it was saturated during the strong seismic motion. S3 was unable to record a seismic acceleration value over 0.25 g, displaying a multi-step function that ranged periodically from 0.25g to -0.25g. On the other hand, the Mod-ζ(var) approach allows computing the acceleration trace related to sensor S3 based on the seismic normalized mode shapes and the modal responses (Figure 17) estimated from other sensors (S1, S2, S4, S5, and S6). As a result, Figure 12 shows the model-predicted acceleration trace estimated from the Mod-ζ(var) approach with a red line. Over it, the saturated seismic signal is also displayed with a blue line. In general, it can be observed that the model-predicted response matched the seismic data during the time intervals when the signal is not saturated (at the beginning and end of

the seismic motion). Moreover, the model-predicted and saturated seismic data (during the strong motion) cross the zero at precisely the same times, showing out-of-phase signals (the saturated signal shows an oppositive sign compared to the model-predicted response). In conclusion, the Mod-ζ(var) approach allows for rebuilding the seismic data related to the saturated sensor S3.

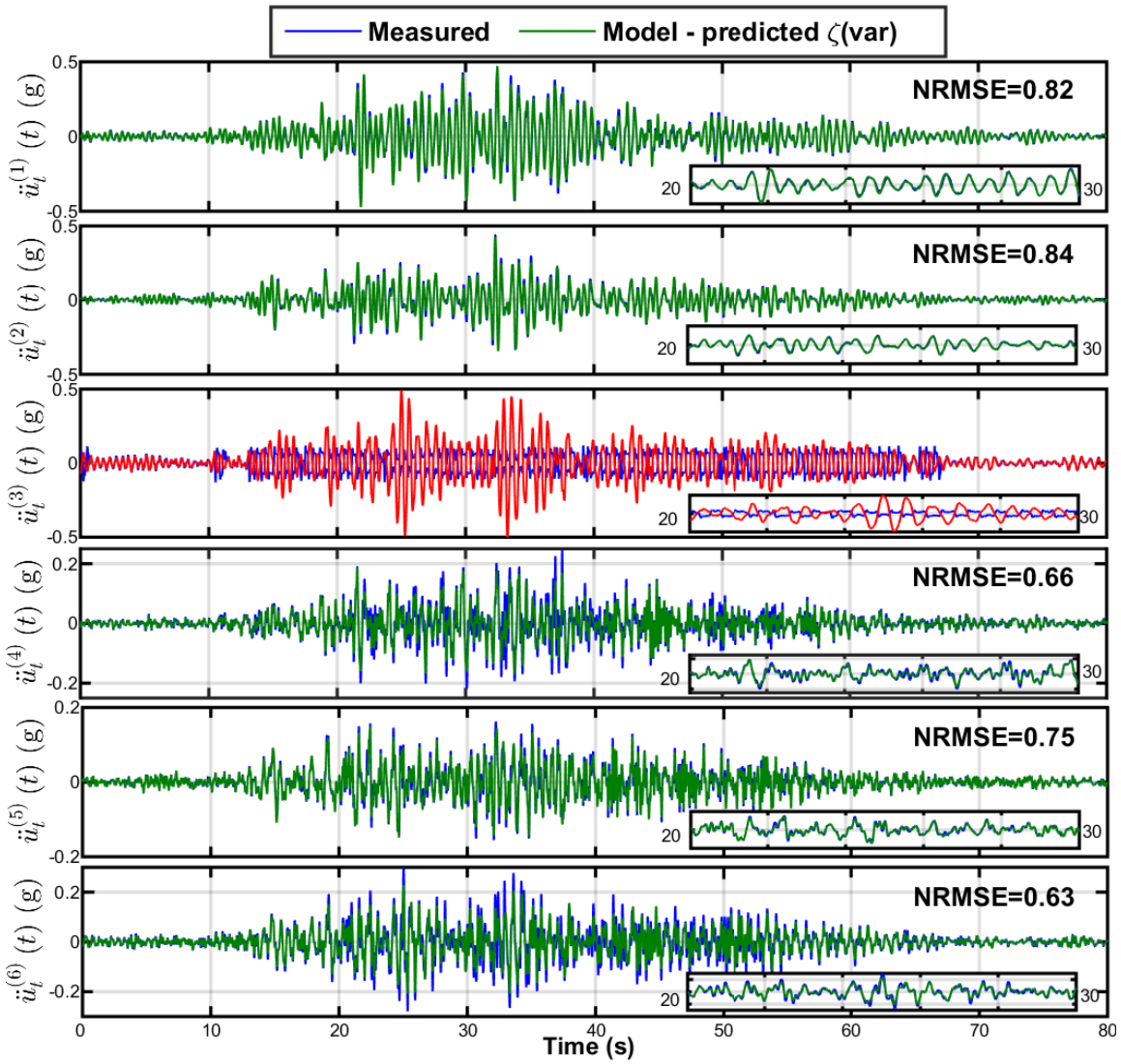

Figure 12: Model-predicted absolute acceleration response (Mod-ζ(var)) vs seismic data related to the 02/27/2010 central Chilean mega-earthquake (Mw=8.8)

Figure 13 compares the PSD in log-scale related to the measured sensor data and their residuals, which are the difference between the measured and the model-predicted absolute acceleration traces. It can be observed that residuals are significantly lower than the measured signals for low frequencies (<7 Hz), implying that low-frequency structural modes were correctly adjusted. S4 and S6 show an imperfect matching for frequencies over 4Hz that can be attributed to errors in estimating the normalized seismic mode shapes at these sensors' positions.

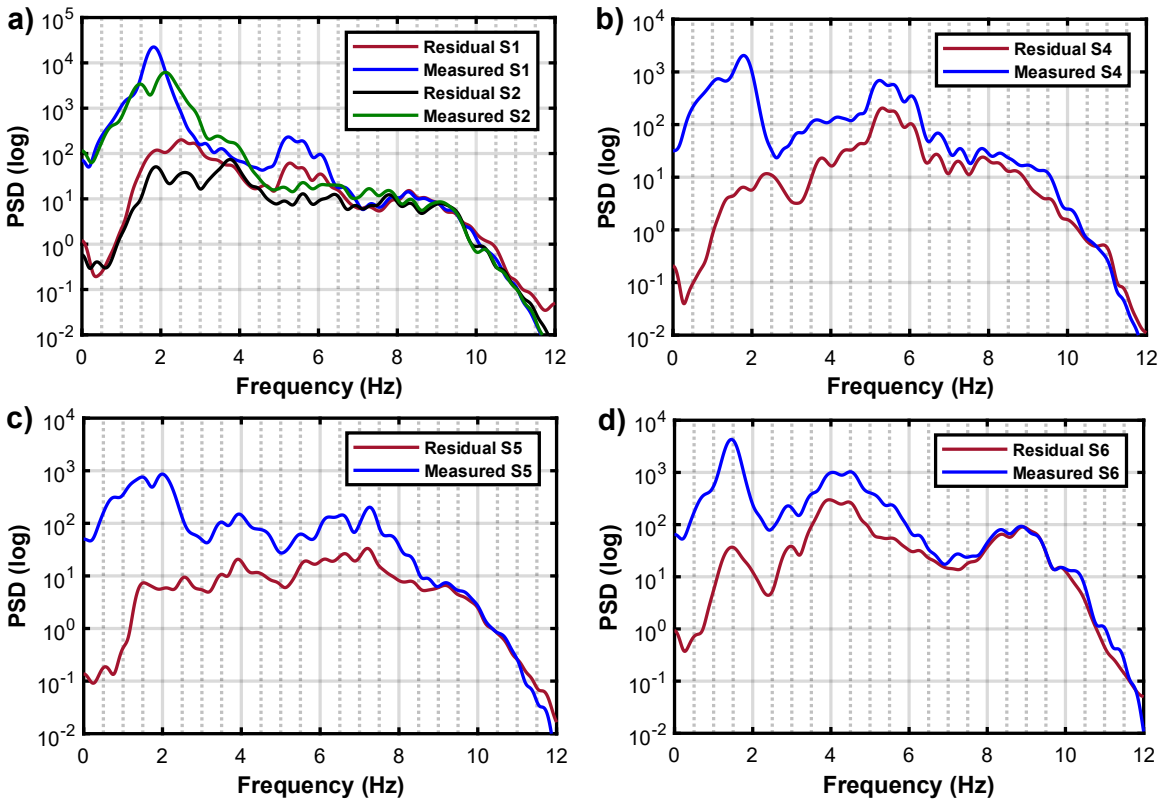

Figure 13: a) PSD for residual and seismic data related to sensors S1 and S2, b) PSD for residual and seismic data related to sensors S4, c) PSD for residual and seismic data related to sensors S5, d) PSD for residual and seismic data related to sensors S6 related to the 02/27/2010 Chilean mega-earthquake (Mw=8.8)

Figure 14 shows the time-variant natural frequencies adjusted by the Mod-ζ(var) approach using color lines. Figure 14 also displays the STTF computed between sensors placed on the eighth floor of the building (S1/S8 refers to longitudinal sensors and S2/S7 to transverse sensors). The STTF plots were computed using a Hanning window of 7 sec. The STTF agreed with the trend of time-variant natural frequencies, which allows verifying the Mod-ζ(var) results. It can be observed that natural frequencies were significantly reduced during the strong phase of the seismic motion. For example, the first natural frequency was 1.99 Hz at the beginning, but it reached a minimum value of 1.37 Hz during the seismic record. Moreover, the natural frequencies were partially recovered at the end of the seismic event. For instance, the first natural frequency finished with a value of 1.51Hz at the end of the seismic analysis. This indicates that the structure experienced residual damage because a permanent reduction of its natural frequencies can be observed. The results were consistent with the differences observed from OMA in Table 1. Furthermore, the natural frequencies related to 1st, 2nd, 3rd, and 5th structural modes were similar to the previously estimated by Carreño [42,43] for the JEAM building subjected to the Chilean mega-earthquake (Mw=8.8).

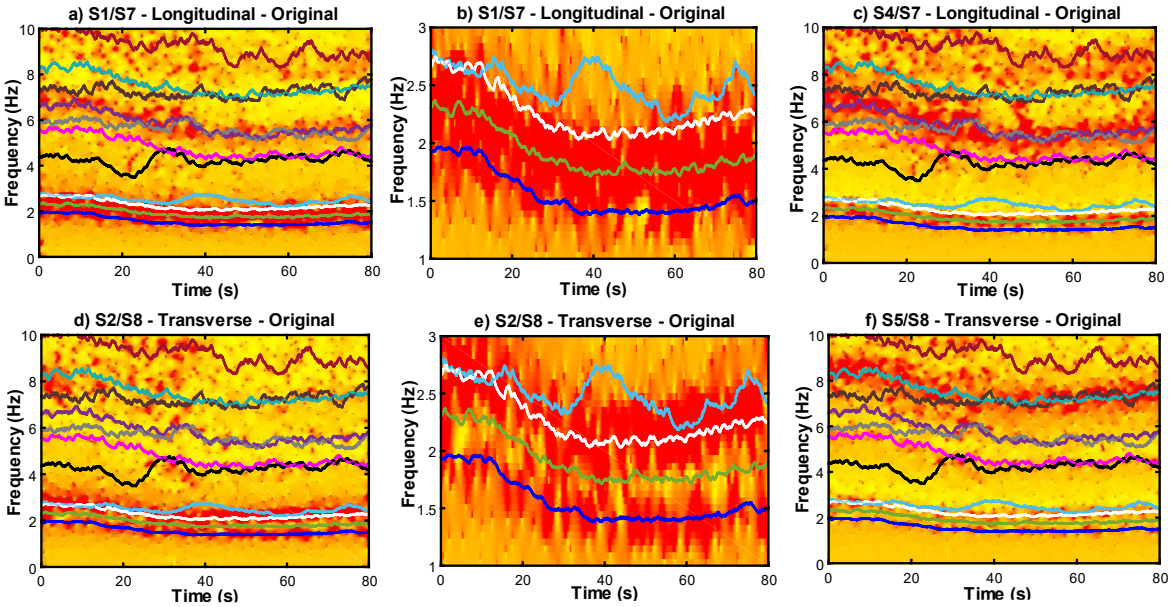

Figure 14: STTF and time-variant natural frequencies estimated by the Mod-ζ(var) approach related to a) S1/S7 seismic data, b) S1/S7 zoom of seismic data, c) S1/S7 seismic data, d) S2/S8 seismic data, e) S2/S8 zoom of seismic data, f) S5/S8 seismic data related to the 02/27/2010 Chilean mega-earthquake (Mw=8.8)

Figure 15 shows the time-variant damping ratios estimated by the Mod-ζ(var) approach with blue lines related to the most relevant structural modes. Datched red lines referred to damping ratios estimated by the DSI method associated with a minor seismic event and indicated in Table 2. As a reference, the damping ratios observed when the peak modal acceleration responses occurred (Figure 17) are also marked with scatter points related to the longitudinal seismic input (S7) and the transverse seismic input (S8). It can be observed that damping ratios showed a global trend to increase during the strong seismic motion phase (10s to 60s). However, they exhibited local variations during the seismic event, which seems consistent with the STTF plots (higher damping ratios relate to larger bandwidths). In contrast to the global trend, local increments of damping ratios caused the reduction of the signal amplitudes, which triggered local increases in natural frequencies. It should be pointed out that damping ratios are described by multiple sources of energy dissipation, such as fluid viscous damping, the hysteretic response of structural elements, frictional interactions, pounding, nonstructural element responses, and soil-structure interactions, among others.

Figure 16 refers to the time variation observed for seismic normalized mode shapes adjusted by the Mod-ζ(var) approach. Figure 16a and Figure 16b show the time-variant average mode contribution (η_{ij})[40]. Similarly, Figure 16c and Figure 16d show the MAC values [54] computed between time-variant mode shapes and their initial values. Figure 16e and Figure 16f show the global mode shape error ($\varepsilon_{modes}{}^{(l)}{}_{j}$) [40] that refers to the mode shape estimation's accuracy on each output because their sum should equal the seismic influence vectors. Both η_{ij} and $\varepsilon_{modes}{}^{(l)}{}_{j}$ were previously defined in [40]; however, they are redefined for the case of Multiple Inputs (MI) as follows,

$$\eta_{ij} = \frac{1}{N_m} \cdot \sum_{l=1}^{N_m} \left| \boldsymbol{\varphi}_{ij}^{(l)}(t_k) \right| \quad ; \quad \varepsilon_{modes}{}^{(l)}{}_j = \frac{\left| \sum_{i=1}^{N_2} \boldsymbol{\varphi}_{ij}^{(l)}(t_k) - \mathbf{r}_j^{(l)} \right|}{\mathbf{r}_j^{(l)}} \tag{5}$$

Where, $\boldsymbol{\varphi}_{ij}^{(l)}(t_k)$ = the seismic normalized mode shape related to the i-th structural mode, the j-th seismic input, and the l-th output DOF. $\mathbf{r}_j^{(l)}$ = the theoretical seismic influence vector (Table 4) at the l-th output DOF related to the j-th seismic input.

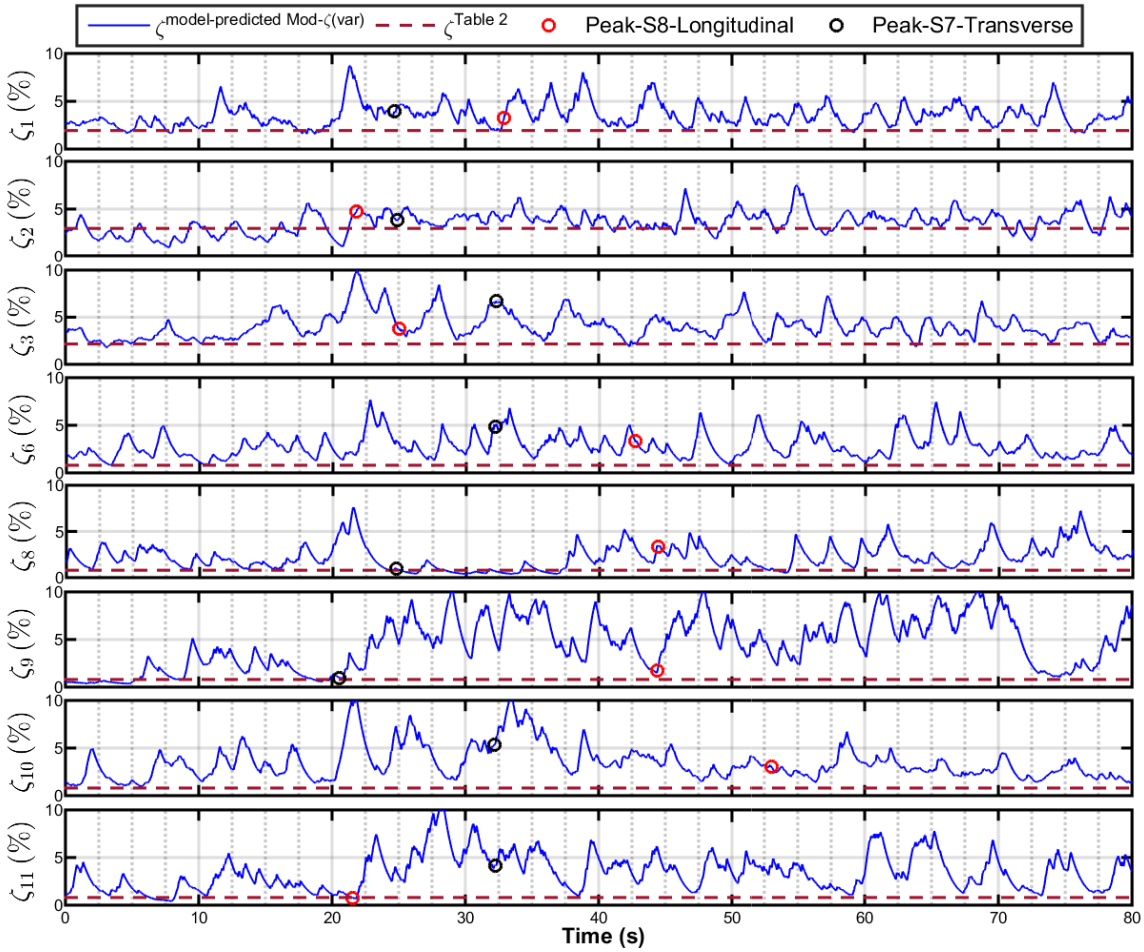

Figure 15: time-variant damping ratios estimated by the Mod-ζ(var) approach related to the 02/27/2010 central Chilean mega-earthquake (Mw=8.8)

Figure 16 allows concluding that mode shapes did not experience significant variations during the mega-earthquake (the lowest MAC value was higher than 0.996). The almost invariant mode shapes are also consistent with the observations discussed in section 3, where mode shapes estimated from OMA before and after the earthquake did not evidence significant variations (Figure 4). Similarly, mode shapes estimated from minor seismic events before and after the mega-earthquake do not show perceptible variations (Table 3). Therefore, it can be concluded that natural frequencies and damping ratios are the dynamic properties that mainly variate during a seismic event, considering that mode shapes can be

virtually invariant if the structure experiences limited damage. Similarly, the average mode contribution shows that the 2nd mode is the most relevant for the longitudinal response associated with the seismic input (S7) acting over the JEAM building. Similarly, the transverse response (related to S8) is mainly influenced by the 1st, 3rd, and 6th structural modes. The global mode shape errors indicate that S4 and S6 present higher errors in estimating normalized mode shapes (or because other structural modes were not considered to describe the response for these sensors). It is worth noting that S4 and S6 are the sensors that exhibit the lower NRMSE values in Figure 12 (i.e., sensors with the worse adjustment).

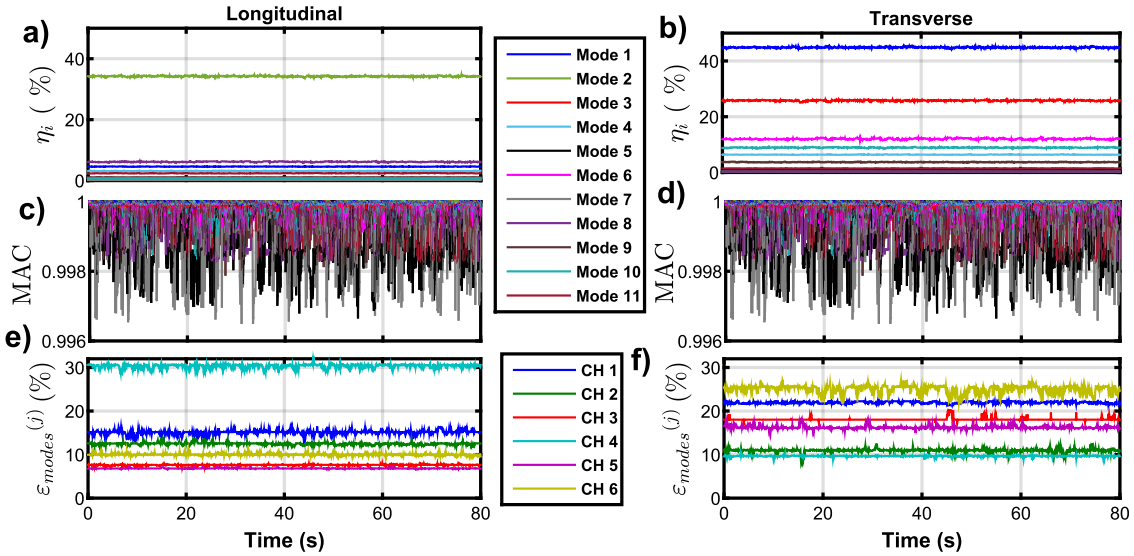

Figure 16: (a,b) Average mode contribution, (c,d) time evolution of MAC values, (e,f) global mode shape error estimated by the Mod-ζ(var) approach related to each seismic input (S8-Longitudinal and S7 Transverse) for the 02/27/2010 central Chilean mega-earthquake (Mw=8.8)

Figure 17 shows the nonlinear modal absolute acceleration response obtained from the Mod-ζ(var) adjustment related to the most participant structural modes along the longitudinal seismic input (S8) and the transverse seismic input (S7), respectively. These modal responses were computed considering time-variant natural frequencies (Figure 14), damping ratios (Figure 15), and their respective seismic inputs (Eq.(4)). It should be pointed out that the modal responses are continuous functions over time based on the Mod-ζ(var) assumptions. Red stems indicate the times and values when each seismic input's peak modal absolute acceleration response occurred. Other nonlinear modal responses, such as relative or absolute modal acceleration, velocities, and displacements, can be directly computed using the Mod-ζ(var) approach.

Based on the peak values of the modal acceleration traces displayed in Figure 17, the Empirical Response Spectrum (ERS) for each seismic input can be determined. The ERSs are graphically represented by joining scatter points with straight lines related to the peak modal responses associated with each structural mode. A scatter point is drawn for each natural frequency. These points are defined by the peak value of the modal response in the ordinate coordinate (e.g., absolute peak acceleration of Figure 17) and the natural period (inverse of natural frequency in Figure 14) that the structural mode exhibits at the time of its peak modal response in the abscissa coordinate (Figure 14).

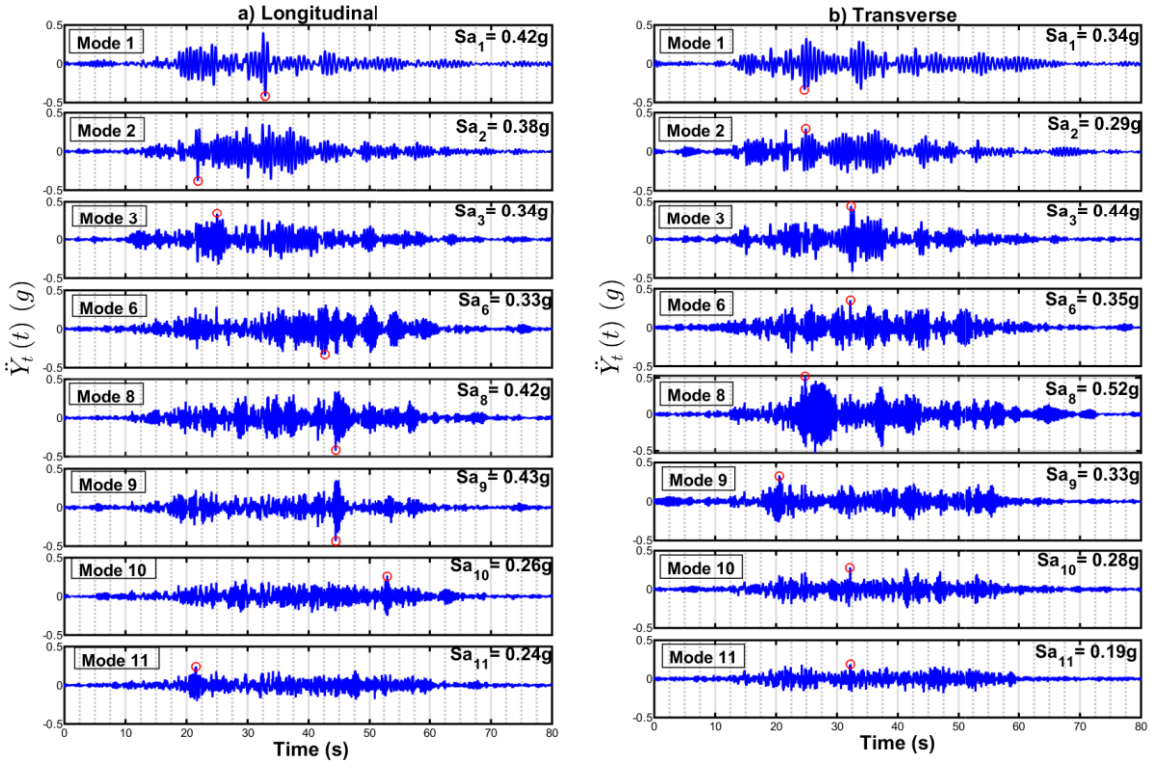

Figure 17: (a) absolute modal acceleration response related to the longitudinal seismic input (S8), (b) absolute modal acceleration response related to the transverse seismic input (S7) for the 02/27/2010 central Chilean mega-earthquake (Mw=8.8)

Figure 18 shows the absolute acceleration and relative displacement response spectra related to the longitudinal (S8) and transverse (S7) seismic inputs. The ERSs are compared with response spectra computed by assuming constant damping ratios (2% in black, 5% red, and 7% green lines) and their respective seismic inputs. The ERSs can only be evaluated for the natural periods of the JEAM building (or those employed in the Mod-ζ(var) approach); therefore, they can only be assessed until the maximum natural period of the JEAM building. It is worth noting that the response spectra for longer natural periods are also shown in adjacent plots. The scatter points are distinguished with different colors to indicate their dominant movement in agreement with Table 2 (i.e., blue refers to Tr-To mode shapes, green to Lo, Red to Lo-To, and cyan to To).

It can be observed that the ERSs (Figure 18) are similar to the response spectrum computed with a damping ratio of 5%, particularly if the spectral values are associated with the excitation direction (e.g., Lo and Lo-To values for the ERS computed with the longitudinal input). This observation validates the damping ratio value commonly employed by different seismic codes worldwide. It should be pointed out that the seismic intensity experienced by the JEAM building can be considered intermediate during the 02/27/2010 central Chilean mega-earthquake (Mw=8.8) with a PGA of 0.15g and 0.17g along the longitudinal and transverse direction, respectively. As a result, the JEAM building experienced reduced damage during the analyzed seismic event. Thus, it can be concluded that a damping ratio of 5% is reasonable for determining the response spectrum of mid-rise 10-story R/C shear-wall buildings that experience low damage.

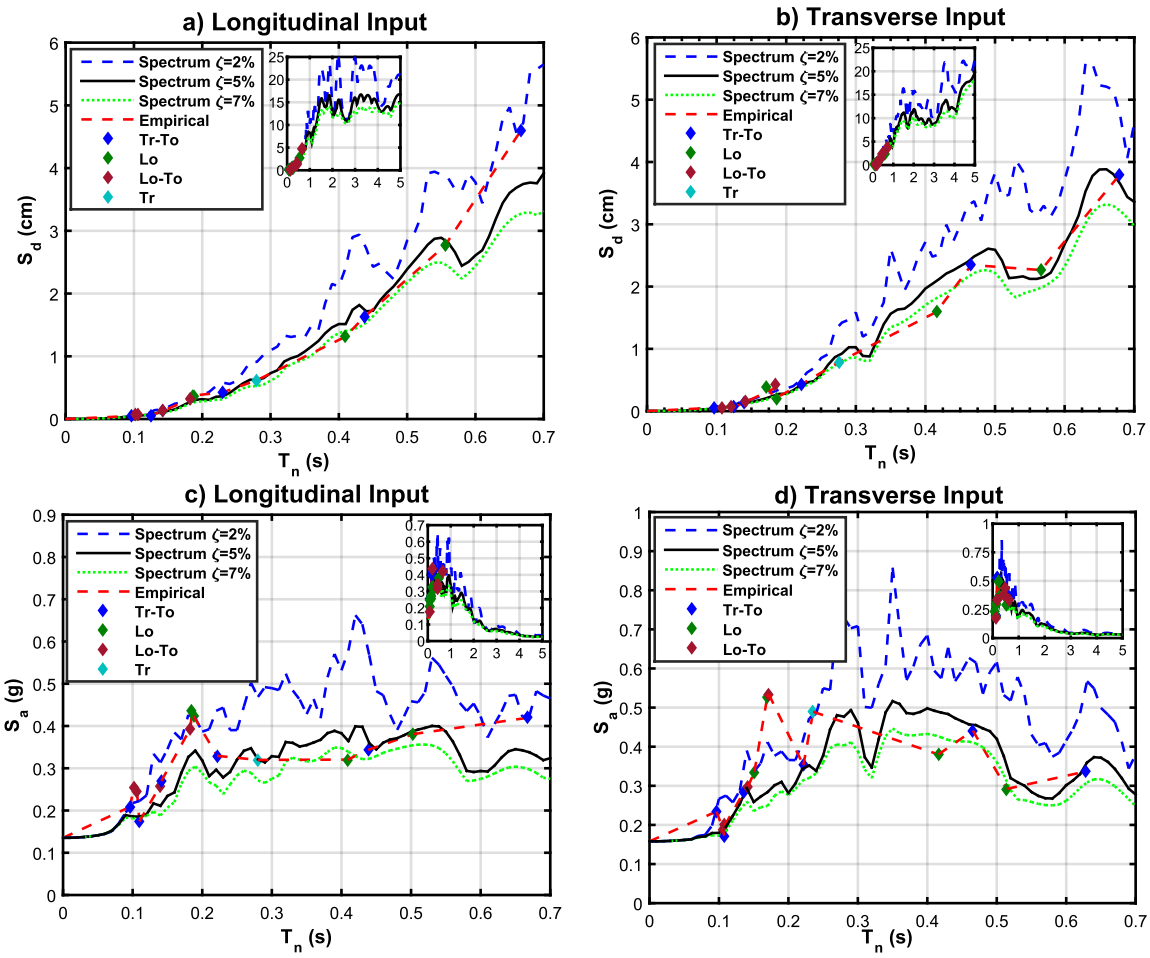

Figure 18: (a) Relative displacement ERS related to the longitudinal (S7) seismic input, (b) Relative displacement ERS related to the transverse (S8) seismic input, (c) Absolute acceleration ERS related to the longitudinal (S7) seismic input, (d) Absolute acceleration ERS related to the transverse (S8) seismic input for the 02/27/2010 central Chilean mega-earthquake (Mw=8.8)

7. INTER-STORY DRIFTS AND LOCAL RESPONSES OF THE JEAM BUILDING FROM ACTUAL SEISMIC DATA

Once the SDOF nonlinear modal responses are estimated by the Mod-ζ(var) (Figure 17), the seismic response of the building can also be evaluated on the unmeasured floors. In other words, unmeasured floor responses can be computed as the product between the seismic normalized mode shapes (for all floors) and the modal responses (Eq.(1)). It should be pointed out that mode shapes have not evidenced significant variation during the mega-earthquake, according to results displayed in Figure 16. Similarly, the MAC values determined between mode shapes estimated from OMA before and after the mega-earthquake do not show significant fluctuations (Figure 4). Therefore, it is reasonable to assume that the seismic response of unmeasured floors can be accurately estimated as the product between the normalized seismic mode shapes determined from OMA and the nonlinear modal responses computed by the Mod-ζ(var) (Figure 17), as it was observed with sensor S3 that was saturated.

The normalized seismic mode shapes for all the building's floors can be estimated from the AV tests presented in section 4. However, a scale factor (α_{ij}) should be applied to the mode shapes estimated from OMA (Figure 5) to transform them into normalized ones for each seismic input. On the one hand, the normalized seismic mode shapes at the sensor positions (3rd and 8th floors) were previously estimated (section 6) from a minor seismic event based on the seismic instrumentation described in section 3. Besides, a geometrical transformation (assuming rigid diaphragms) can be applied to determine the modal displacement at the center of gravities and the four corners of each floor. This geometrical transformation is applied to the scaled OMA's mode shapes (for all floors) and the normalized seismic mode shape (on the 3rd and 8th floors). Then, the scale factor required to transform OMA's mode shapes is fitted, so the OMA scaled mode shape matches the normalized seismic mode at the four corners for the 3rd and 8th floors. It enables estimating the scale factor that should be applied to OMA's mode shapes to generate the normalized seismic mode shapes for all the building's floors.

Once the seismic response of measured and unmeasured floors was computed, inter-story drift ratios of the geometrical center or any point on the plan could be calculated. Figure 19 shows the peak values over time of inter-story drifts computed at the geometrical centers of the JEAM building (longitudinal, transverse) related to the 02/27/2010 central Chilean mega-earthquake (Mw=8.8). It can be observed that the higher inter-story drifts are generated at the 7th story. It can be explained because the principal mode shapes (1st, 2nd, 3rd) estimated from OMA (Figure 5) showed higher drift deformation at the upper levels, consequent with a mode shape of a bending cantilever beam. The drift ratios computed from idealistic FEM (section 5) are compared. Overall, it can be observed that the Mod-ζ(var) drift ratios are higher than FEM. The differences occurred because the structures experienced stiffness degradation during the seismic event exhibiting lower natural frequencies than the FEM. Therefore, different spectral values are observed (Figure 9) because the natural frequencies determined during the seismic event (Figure 14) were significantly different from those obtained from the idealistic FEM (Table 1). For example, the first longitudinal natural period obtained from the FEM was 0.27s (Table 1); in contrast, the actual one observed at the peak modal response was 0.56s (Figure 18), implying that the modal displacement is reduced from 2.8cm to 0.6cm (Figure 18), i.e., a scale factor of 4.7. Similarly, the first transverse mode has a natural period of 0.41s for the FEM and 0.68s based on the Mod-ζ(var) results, implying that the modal displacement was reduced from 3.8cm to 2cm (Figure 18), implying a scale factor of 1.9. These differences indicate that the FEM stiffness (e.g., the modulus of elasticity) should be reduced to 25-35% of the FEM uncracked value to obtain natural frequencies similar to those observed during the seismic event.

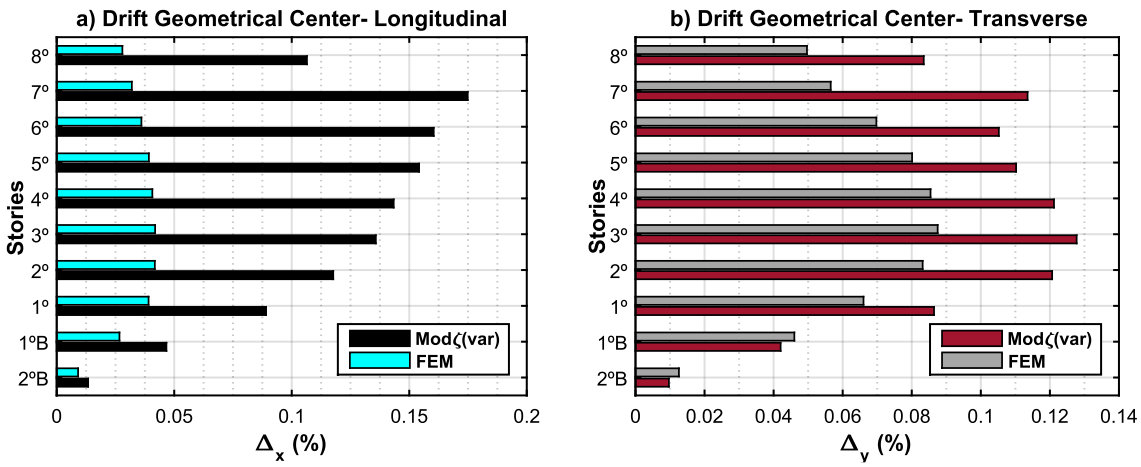

Figure 19: Peak inter-story drift related to each direction of analysis for the JEAM building associated with the 02/27/2010 central Chilean mega-earthquake (Mw=8.8) a) longitudinal direction based on Mod-ζ(var) and FEM results, b) transverse direction based on Mod-ζ(var) and FEM results.

The computed measured and unmeasured floor movements were applied to the FEM of the JEAM building detailed in section 5, observing that rigid diaphragms were modeled for each deck. The floor movements were applied using a multiple seismic support analysis (if the FEM software allows this option). Alternatively, dashpots with high damping constant values (or springs) can be added to the geometrical centers and apply forces equal to the product between the model-predicted time-history relative velocities (or displacements) and the assigned damper (or spring) constants. Before performing the time-history analysis, the seismic weight of the building might be applied to evaluate the internal forces correctly. Therefore, this analysis allows for generating the genuine deformation experienced by the JEAM building during the mega-earthquake. As a result, the FEM can be employed to determine the local deformation of elements (e.g., frames, shells, solid, nonlinear components, etc.) and determine their internal forces, strains, or stresses (including local strains related to steel bars or concrete fibers). The computation of internal forces, strain, and stresses will be accurate if a nonlinear model of the element is considered while it experiences deformation over its yielding limit. Linear elements can also be employed if strains are lower than their yielding strains. In this context, Figure 20 shows the peak drift ratios experienced by Wall 1L, Wall 2L, Wall 1T, and Wall 2T (whose distribution is described in Figure 3) over time. Figure 21 shows the same values but computed using the idealistic FEM detailed in section 5, which allows comparison with the actual deformations obtained from the Mod-ζ(var). It is noted that the Mod-ζ(var) shows higher values than FEM because of the difference in the natural frequencies discussed before. The drift ratios obtained from FEM and Mod-ζ(var) tend to increase with height, similar to a bending cantilever beam. However, significant differences are observed on the top stories, indicating that the top level experience a whipping lash effect. This effect could be caused by an unknown mass concentration or stiffness degradation experienced on the top stories.

The FEM drift ratios (Figure 21) suggest that structural walls are far from reaching the Immediate Occupance (IO) limit (0.40% according to FEMA 356 [59] or 0.50% according to the Chilean recommendations [60]); therefore, the structure should not have been

experienced structural damage. Nevertheless, these results disagree with the significant variation of natural frequencies experienced by the building during the mega-earthquake (Figure 14 and Table 1). On the other hand, the Mod-ζ(var) drift ratios (Figure 20) are slightly lower than the IO limit. Thus, the results are consistent with the permanent reduction of natural frequencies exhibited before and after the mega-earthquake by the JEAM building (~20% reduction according to Table 1), considering that R/C walls can experience a stiffness degradation between 20-30% when they are subjected to a drift ratio of 0.2%-0.3%, according to [61]. Finally, the Mod-ζ(var) drift ratios are consistent with micro-cracks observed on structural walls and nonstructural components observed after the earthquake.

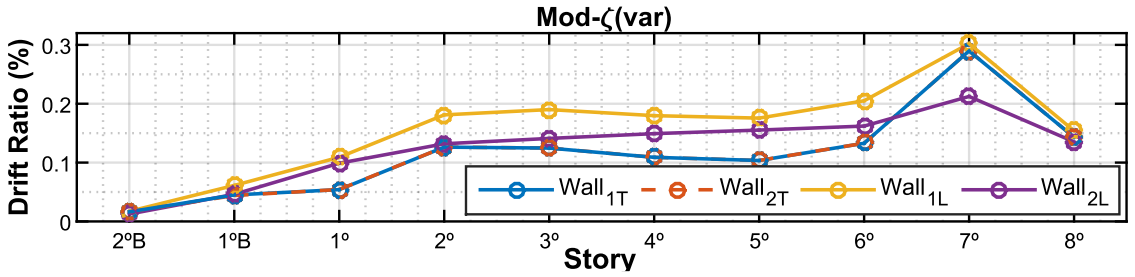

Figure 20: Inter-story drift ratios for Wall 1L, Wall 2L, Wall 1T, and Wall 2T determined from the Mod-ζ(var) approach.

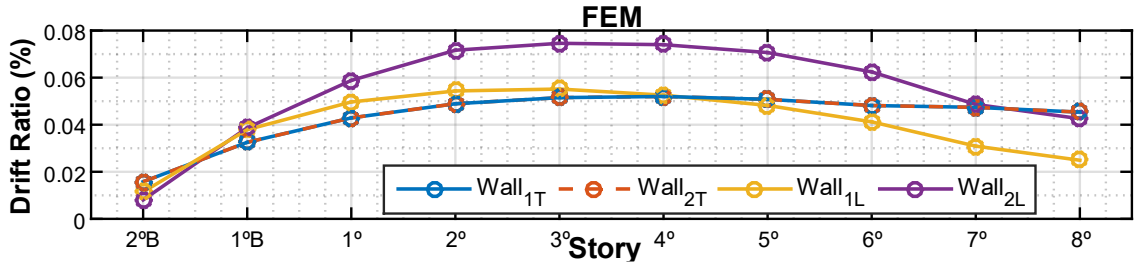

Figure 21: Inter-story drift ratios for Wall 1L, Wall 2L, Wall 1T, and Wall 2T determined from the idealistic FEM.

Figure 22 shows the peak values of the curvatures determined for Wall 1L, Wall 2L, Wall 1T, and Wall 2T based on the Mod-ζ(var) results. Similarly, Figure 23 displays curvature obtained with the idealistic FEM. It can be observed that both show that the higher curvatures are generated on the 2º basement, noting that high curvatures are also developed on the top stories. Again, the Mod-ζ(var) shows higher values than FEM, explained by the difference in natural frequencies. It should be pointed out that the curvature values imply that there is no damage due to bending, considering that the moment-curvature plots obtained for analyzed walls indicate that yielding occurs to a curvature value of 0.0025.

The inter-story shear forces of the building can be computed as the cumulative product between the absolute acceleration and the floor masses at their center of gravity. Therefore, floor masses (and their center of gravities) were directly extracted from the FEM (i.e., the mass distribution is assumed to be correctly computed by the FEM). Then, the absolute accelerations on the floors' center of gravities are calculated using a geometrical transformation from responses computed from the Mod-ζ(var) results. Figure 24 shows the peak values of the inter-story shear forces along the longitudinal and transverse directions over time. It can be observed that the inter-story shear forces obtained from the Mod-ζ(var)

are smaller than the determined from the FEM. It occurs because the modal accelerations associated with higher frequencies are more considerable than the computed for lower natural frequencies (Figure 18).

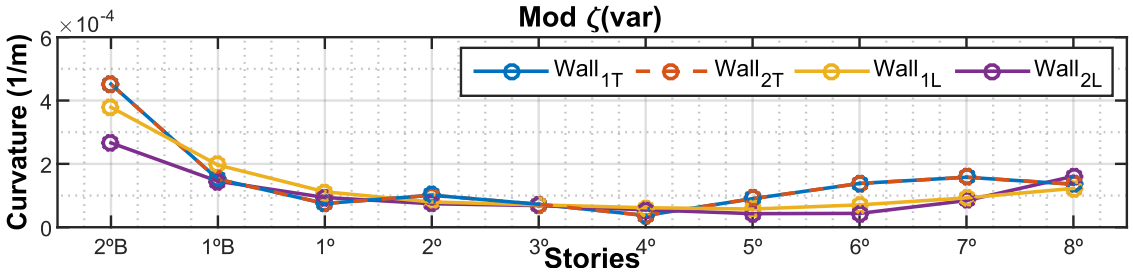

Figure 22: Curvature for Wall 1L, Wall 2L, Wall 1T, and Wall 2T determined from the Mod-ζ(var) approach.

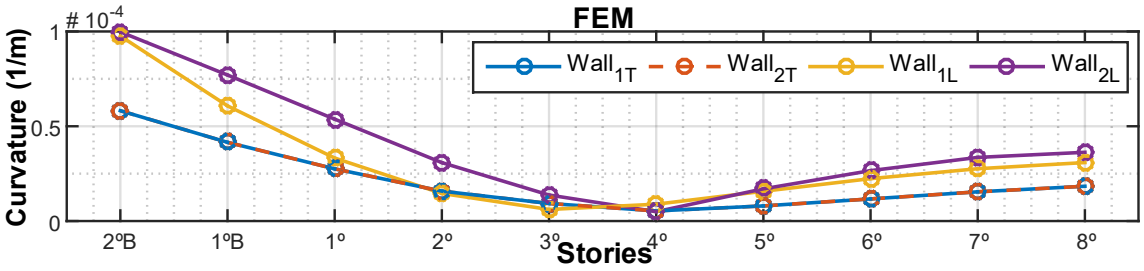

Figure 23: Curvature for Wall 1L, Wall 2L, Wall 1T, and Wall 2T determined from the idealistic FEM.

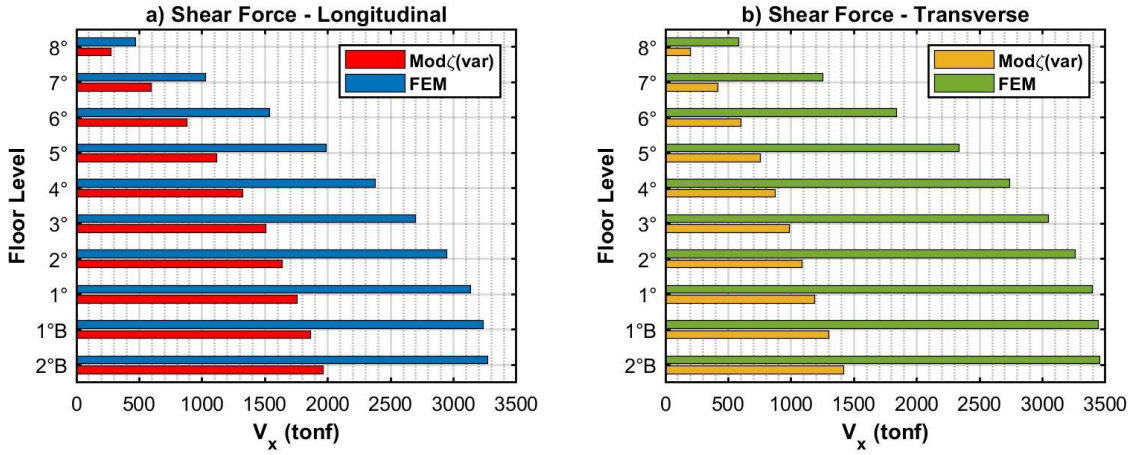

Figure 24: Peak inter-story forces related to each direction of analysis for the JEAM building associated with the 02/27/2010 central Chilean mega-earthquake (Mw=8.8)

8. CONCLUSIONS

The Mod-ζ(var) approach was formulated, implemented, and validated to study the seismic response of 3D buildings subjected to multiple seismic inputs. This approach uses nonlinear modal responses to match seismic data and adjusts time-varying modal parameters through small data windows. This enables the determination of the empirical response spectrum (ERS) related to each seismic input.

The JEAM building's mode shapes, determined from AV tests for all floors, can be combined with the nonlinear modal responses obtained from the Mod-ζ(var) approach to compute the

seismic response of measured and unmeasured floors. Overall, the mode shapes remained similar before, during, and after the mega-earthquake, resembling a bending cantilever beam. The top floors are highly influenced by low-frequency modes, resulting in longer drift ratios, while higher curvatures are generated at the bottom levels, observing that the seismic response of bottom floors can be significantly affected by high-frequency modes. The OMA's mode shapes coincide with the seismic case relative to the base, with only small displacements observed for high-frequency modes (>5Hz), suggesting that Soil-Structure-Interaction has a minimal impact on the JEAM building's dynamic properties.

The Mod-ζ(var) approach was successfully applied to simulated data obtained from a FEM of the JEAM building, accurately estimating the time-variant natural frequencies and damping ratios for the analytical case. The approach is deemed reliable for linear structures under multiple seismic inputs and practical in determining empirical response spectra, as the estimated values coincide with the computed response spectra from seismic inputs applied to the base for each direction of analysis.

The Mod-ζ(var) approach was used to evaluate the JEAM building seismic performance during the central Chilean mega-earthquake (Mw=8.8), revealing that mode shapes did not change significantly over time. Natural frequencies showed variability even for small seismic events, with initial and final values coinciding with OMA values but decreasing rapidly at the beginning of seismic events (<0.005g). During the mega-earthquake, natural frequencies showed a progressive reduction, with a peak decrease of 30%, partially recovering at the end of the event, leaving a residual decrease of 20%. These variations were consistent with the changes observed from OMA before and after the earthquake. Damping ratios were highly variable over time, with a trend towards higher values during the strong motion phase. Surprisingly, local damping ratio increments caused attenuation of the response, resulting in locally recovered natural frequencies (higher values). Despite the high variation of damping ratios, the ERSs are similar to the response spectra computed with a damping ratio of 5%, validating the commonly employed value for design purposes, at least for R/C shear wall buildings subjected to intermediate seismic demands.

The building's floor movements were applied to a FEM, focusing on studying drift ratios and curvatures of relevant walls. Results show that drift ratios range from 0.1% to 0.3%, indicating low structural damage (approaching but not exceeding the Immediate Occupance limit of 0.4%-0.5%), implying a stiffness degradation of 20-30%. These results are consistent with variations in natural frequencies observed through OMA and seismic analysis. Although walls experienced stiffness degradation due to the opening of minor cracks, they become closed by the building's self-weight. Similarly, strength and ductility remained almost unchanged, indicating that the building has not experienced practical damage; however, it exhibited a permanent reduction of its initial natural frequencies. Higher wall curvatures were observed at the bottom levels but cannot be attributed to damage.

9. ACKNOWLEDGMENT

The authors acknowledge the financial support from the Chilean National Agency for Research and Development (ANID) through the research grant FONDECYT 1200277.

10. BIBLIOGRAPHY

[1] Kim J, Lynch JP. Subspace system identification of support-excited structures—part I: theory and black-box system identification Junhee. Earthq Eng Struct Dyn 2012;41:1549–68. doi:10.1002/eqe.2184.

[2] Van Overschee P, De Moor B. Subspace Identification for Linear System: Theory - Implementation - Applications. Kluwere Academic Publishers; 1996.

[3] Shin CY, Tsuei YG, Allemang RJ, Brown DL. Complex and Mode Indication Function and Its Applications to Spatial Domain Parameter Estimation. Mech Syst Signal Process 1988;2:367–77.

[4] Loh C-H, Chen J-D. Tracking modal parameters from building seismic response data using recursive subspace identification algorithm. Earthq Eng Struct Dyn 2017;46:2163–83. doi:10.1002/eqe.2900.

[5] Adams D, Farrar C. Classifying Linear and Nonlinear Structural Damage Using Frequency Domain ARX Models. Struct Heal Monit 2002;1:185–202. doi:10.1177/1475921702001002005.

[6] Fassois SD. MIMO LMS-ARMAX identification of vibrating structures-Part I: The method. Mech Syst Signal Process 2001;15:723–35. doi:10.1006/mssp.2000.1382.

[7] Ulusoy H, Feng MQ, Fanning PJ. System identification of a building from multiple seismic records. Earthq Eng Struct Dyn 2011;40:661–74. doi:10.1002/eqe.1053.

[8] Juang JN, Phan M, Horta LG, Longman RW. Identification of observer/kalman filter markov parameters - theory and experiments. J Guid Control Dyn 1993;16:320–9. doi:10.2514/3.21006.

[9] Siringoringo DM, Fujino Y. System identification applied to long-span cable-supported bridges using seismic records. Earthq Eng Struct Dyn 2008;37:361–86. doi:10.1002/eqe.758.

[10] Siringoringo DM, Fujino Y. Observed dynamic performance of the Yokohama-Bay Bridge from system identification using seismic records. Struct Control Heal Monit 2006;13:226–44. doi:10.1002/stc.135.

[11] Li Y, Mau ST. A case study of mimo system identification applied to building seismic records. Earthq Eng Struct Dyn 1991;20:1045–64. doi:10.1002/eqe.4290201106.

[12] Beck JL, Jennings PC. Structural identification using linear models and earthquake records. Earthq Eng Struct Dyn 1980;8:145–60. doi:10.1002/eqe.4290080205.

[13] Chaudhary MTA, Abé M, Fujino Y, Yoshida J. System identification of instrumented bridge using earthquake-induced record. J Struct Eng 2000;126:1187.

doi:10.1061/(ASCE)0733-9445(2000)126.

[14] Chen HM, Qi GZ, Yang JCS, Amini F. Neural network for structural dynamic model identification. J Eng Mech 1995;121:1377–81. doi:10.1061/(ASCE)0733-9399(1995)121:12(1377).

[15] He J, Fu Z-F. Modal Analysis. Butterworth Heinemann; 2001.

[16] Rahmani M, Todorovska MI. 1D system identification of buildings during earthquakes by seismic interferometry with waveform inversion of impulse responses-method and application to Millikan library. Soil Dyn Earthq Eng 2013;47:157–74. doi:10.1016/j.soildyn.2012.09.014.

[17] Hernández F, Díaz P, Astroza R, Ochoa-Cornejo F, Zhang X. Time variant system identification of superstructures of base-isolated buildings. Eng Struct 2021;246. doi:10.1016/j.engstruct.2021.112697.

[18] The MathWorks Inc. MATLAB 2014b 2014.

[19] Risuleo RS, Bottegal G, Hjalmarsson H. Approximate Maximum-likelihood Identification of Linear Systems from Quantized Measurements∗. IFAC-PapersOnLine 2018;51:724–9. doi:10.1016/j.ifacol.2018.09.169.

[20] Caravani P, Watson ML, Thomson WT. Recursive Least-Squares Time Domain Identification of Structural Parameters. J Appl Mech 1977:135–40.

[21] Chu S-Y, Lo S-C. Application of the on-line recursive least-square method to perform structural damage assessment. Struct Control Heal Monit 2011;18:241–64. doi:10.1002/stc.

[22] Astroza R, Ebrahimian H, Conte JP. Material parameter identification in distributed plasticity FE models of frame-type structures using nonlinear stochastic filtering. J Eng Mech 2015;141:1–17. doi:10.1061/(ASCE)EM.1943-7889.0000851.

[23] Graf W, Freitag S, Kaliske M, Sickert JU. Recurrent Neural Networks for Uncertain Time-Dependent Structural Behavior. Comput Civ Infrastruct Eng 2010;25:322–3. doi:10.1111/j.1467-8667.2009.00645.x.

[24] Ahmadlou M, Adeli H. Enhanced probabilistic neural network with local decision circles: A robust classifier. Integr Comput Aided Eng 2010;17:197–210. doi:10.3233/ICA-2010-0345.

[25] Reuter U, Möller B. Artificial Neural Networks for Forecasting of Fuzzy Time Series. Comput Civ Infrastruct Eng 2010;25:363–74. doi:10.1111/j.1467-8667.2009.00646.x.

[26] Freitag S, Graf W, Kaliske M. Recurrent neural networks for fuzzy data. Integr Comput Aided Eng 2011;18:265–80. doi:10.3233/ICA-2011-0373.

[27] Adeli H, Karim A. Neural Network Model for Optimization. J Struct Eng 1997;123:1535–43.

[28] Adeli H, Park HS. A neural dynamics model for structural optimization-Theory. Comput Struct 1995;57:383–90. doi:10.1016/0045-7949(95)00048-L.

[29] Park HS, Adeli H. Distributed Neural Dynamics Algorithms for Optimization of Large Steel Structures. J Struct Eng 1997;123:880–8. doi:10.1061/(asce)0733-9445(1997)123:7(880).

[30] Kim H, Adeli H. Discrete cost optimization of composite floors using a floating-point genetic algorithm. Eng Optim 2001;33:485–501. doi:10.1080/03052150108940930.

[31] Lee Y, Wei CH. A computerized feature selection method using genetic algorithms to forecast freeway accident duration times. Comput Civ Infrastruct Eng 2010;25:132–48. doi:10.1111/j.1467-8667.2009.00626.x.

[32] Baraldi P, Canesi R, Zio E, Seraoui R, Chevalier R. Genetic algorithm-based wrapper approach for grouping condition monitoring signals of nuclear power plant components. Integr Comput Aided Eng 2011;18:221–34. doi:10.3233/ICA-2011-0375.

[33] Chabuk T, Reggia J, Lohn J, Linden D. Causally-guided evolutionary optimization and its application to antenna array design. Integr Comput Aided Eng 2012;19:111–24. doi:10.3233/ICA-2012-0395.

[34] Plevris V, Papadrakakis M. A Hybrid Particle Swarm-Gradient Algorithm for Global Structural Optimization. Comput Civ Infrastruct Eng 2011;26:48–68. doi:10.1111/j.1467-8667.2010.00664.x.

[35] Cohen L. Time Frequency Analysis - Theory and Applications 1994.

[36] Huang NE, Shen Z, Long SR, Wu MC, Shih HH, Zheng Q, et al. The empirical mode decomposition and the Hilbert spectrum for nonlinear and non-stationary time series analysis. R Soc London 1998;454:903–95. doi:10.1098/rspa.1998.0193.

[37] Chiu CK. An Introduction to Wavelets. 1st Editio. San Diego, CA, USA: Academic Press Professional, Inc.; 1992.

[38] Diaz P. Análisis de estructuras aisladas con el método de múltiples sub-estructuras (In Spanish). Universidad de Chile, 2018.

[39] Arrochas A. Identificación de las propiedades dinámicas de un estanque de nivel de agua variable (In Spanish). Universidad de Chile, 2019.

[40] Hernández F, Astroza R, Beltrán JF, Zhang X, Mercado V. A experimental study of a cable-pulleys spring-damper energy dissipation system for buildings. J Build Eng 2022;51:104034. doi:10.1016/j.jobe.2022.104034.

[41] Hernandez F, Astroza R, Beltrán JF, Belmar L. A Damper-Spring Device for Seismic Energy Dissipation. 17th World Conf. Earthq. Eng. 17th, 2020, p. 1–12.

[42] Boroschek RL, Carreno RP. Period variations in a shear wall building due to earthquake shaking. SHMII-5 2011 - 5th Int Conf Struct Heal Monit Intell Infrastruct 2011.

[43] Carreño R. Variación de propiedades dinámicas del edificio de la Cámara Chilena de la Construcción: caso sísmico (In Spanish). University of Chile, 2009.

[44] Brincker R, Zhang L, Andersen P. Modal identification of output-only systems using frequency domain decomposition. Smart Mater Struct 2001;10:441–5. doi:10.1088/0964-1726/10/3/303.

[45] Denisse Espinoza. La faceta más personal de Justicia Espada, primera mujer ingeniera de Chile, ve la luz en plataforma digital (In Spanish). Univ Chile 2022:1–2. https://www.uchile.cl/noticias/184879/la-faceta-personal-de-justicia-espada-primera-ingeniera-del-pais.

[46] Bustos J, Pastén C, Pavez D, Acevedo M, Ruiz S, Astroza R. Two-dimensional simulation of the seismic response of the Santiago Basin, Chile. Soil Dyn Earthq Eng 2023;164. doi:10.1016/j.soildyn.2022.107569.

[47] Yáñez Celedón, & Boroschek Krauskopf R. Implementation of continuous monitoring network, dynamic parameters identification system of a shear-wall building. Civ Eng Thesis Univ Chile 2009.

[48] Boroschek R, Aguilar A, León P. Structural health monitoring using strong and weak earthquake motions. NCEE 2014 - 10th US Natl Conf Earthq Eng Front Earthq Eng 2014. doi:10.4231/D3SQ8QJ2C.

[49] Boroschek R, Tamayo F, Aguilar R. Evaluation of the environmental effects on a medium rise building. 7th Eur Work Struct Heal Monit EWSHM 2014 - 2nd Eur Conf Progn Heal Manag Soc 2014:2091–8.

[50] Boroschek R, Núñez T, Yáñez T. Development of a Real Time Internet Based Monitoring System in a Nine Story, Shear Wall building. 14th Eur Conf Earthq Eng 2010:2009.

[51] Bendat JS, Piersol AG. Random Data. Analysis and Measurement Procedures. Fourth Edi. John Wiley & Sons, Inc., Hoboken, New Jersey; 1971. doi:10.2307/2289430.

[52] Boroschek R, Aguilar A, Basoalto J, León P. Structural health monitoring of a mid height building in Chile. 5th Int Oper Modal Anal Conf IOMAC 2013 2013:1–10.

[53] Rahmani M, Hao T-Y, Todorovska M, Boroschek R. STRUCTURAL HEALTH MONITORING OF TORRE CENTRAL BY THE WAVE METHOD. 16th World Conf. Earthquake, 16WCEE 2017, 2017.

[54] Allemang RJ, Brown DL. A correlation coefficient for modal vector analysis. First Int Modal Anal Conf 1982:110–6.

[55] Computer & Structures Inc. CSI Analysis Reference Manual For SAP2000, ETABS, SAFE and CSiBridge. Berkeley, California, USA: 2015.

[56] Roselli I, Malena M, Mongelli M, Cavalagli N, Gioffrè M, De Canio G, et al. Health assessment and ambient vibration testing of the "Ponte delle Torri" of Spoleto during the 2016–2017 Central Italy seismic sequence. J Civ Struct Heal Monit 2018;8:199–216. doi:10.1007/s13349-018-0268-5.

[57] Orlowitz E, Andersen P, Brandt A. Comparison of simultaneous and multi-setup measurement strategies in operational modal analysis. 6th Int Oper Modal Anal Conf

IOMAC 2015 2015.

[58] Clough RW, Penzien J. Dynamics of Structures, Third Edition. 2013. doi:10.1002/9781118599792.

[59] FEMA 356. Prestandard and Commentary for the Seismic Rehabilitation of Buildings. 2000.

[60] ACHISINA. Diseño Sísmico Basado en Desempeño, Un Procedimiento Alternativo para el Análisis y Diseño Sísmico de Edificios (In Spanish). 2017.

[61] Ni X, Cao S, Li Y, Liang S. Stiffness degradation of shear walls under cyclic loading: experimental study and modelling. vol. 17. Springer Netherlands; 2019. doi:10.1007/s10518-019-00682-5.